Fused Deposition Modeling of Composite Reinforced by Continuous Ultra-High Molecular Weight Polyethylene Fiber

Renjie Song

A thesis

submitted in partial fulfillment of the

requirements for the degree of

Master of Science

University of Washington

2023

Committee:

Dwayne Arola

Guozhong Cao

Program Authorized to Offer Degree:

Materials Science and Engineering

University of Washington

Abstract

Fused Deposition Modeling of Composite Reinforced by Continuous Ultra-High Molecular Weight Polyethylene Fiber

Renjie Song

Chair of the Supervisory Committee:
Dwayne Arola
Department of Materials Science and Engineering

Fused Deposition Modeling (FDM) of composites with compliant high-strength fibers could expand opportunities for the design and fabrication of complex compliant structures. However, this area of additive manufacturing (AM) is currently not reported in the open literature. This study pursued developing an approach for creating filaments of continuous ultra-high molecular weight polyethylene fiber tow embedded in a matrix of polycaprolactone (Dyneema/PCL) and successful 3D printing. The microstructure and mechanical properties of the filament were evaluated in terms of key parameters including the fiber distribution (dispersed vs. bundled) and printing condition (before and after FDM). At a minimum fiber volume fraction of 18%, the filament exhibited an ultimate tensile strength (UTS) of 588 ± 41 MPa prior to printing, with apparent fiber strength of 3.2 GPa. For the printed condition, the UTS reached 474 ± 62 MPa and with apparent fiber strength of 2.6 GPa. Fiber dispersion in the filament plays an important role in the printed properties and potential for fiber degradation. Nevertheless, the strength of the

Dyneema/PCL represents a new performance benchmark for compliant composites produced by FDM. This new material system can support applications where strength and toughness are key performance metrics in addition to flexibility.

Table Of Contents

Acknowledgments

First, I would like to thank Dr. Dwayne Arola for all the guidance and support. As a great academic and professional mentor, he taught me a lot about how to become a successful researcher and engineer with self-motivation and great dedication in my career. Additionally, I would like to thank Dr. Guozhong Cao for being a part of my defense committee. A special thank you to Colin Marquis for his help and work on the project based on which I completed this document, and other alumni graduated from the same group: Andy Luong and Sarah Wadell. This work would not have been possible without the help of other members of the Arola group and the MSE department, thank you all for your time and efforts. During these two years for me to complete this Master's program, I received endless support and encouragement from my family, my girlfriend Zhuoying Wei, and my friends, I feel spoiled and cannot appreciate you more, thank you so much for always standing by my side.

Chapter 1 - Introduction

Nowadays, composites have become a fundamental material in a wide range of applications, seeing widespread adoption across a myriad of industries. Their rising prominence can be attributed to an inherent versatility: the ability to engineer specific properties by intentionally selecting from an almost unlimited range of material combinations and processing metrics. This characteristic allows industries to tailor composites to meet specific demands, whether it is enhancing the tensile strength for aerospace applications, improving thermal conductivity for electronics, or achieving the right balance of flexibility and durability for sports equipment. The beauty of composites lies in this adaptability, ensuring that as technological demands evolve, so too can the materials that meet them.

As a manufacturing technology that also offers unlimited freedom for material selection, Additive Manufacturing (AM) has been brought to attention. Unlike conventional manufacturing processes which often constrain design possibilities due to material compatibility and process limitations, AM operates in a realm where these boundaries are vastly expanded, as the manufacturing setup can be easily adjusted accordingly. The inherent layer-by-layer manufacturing concept of AM allows for the incorporation of diverse materials in unique combinations and configurations.

The exploration of new composite material systems for Additive Manufacturing (AM) is not merely a scientific curiosity; it is a pressing imperative. As industries continuously push the boundaries of achievable material properties based on special needs, there is an unending quest for materials that are stronger, lighter, more durable or possess novel functionalities. AM, with its promise of design and material freedom, serves as an ideal platform for this exploration.

Furthermore, the iterative nature of AM—where designs can be rapidly prototyped, tested, and refined—means that the integration and assessment of new material systems can be expedited. With AM, a design modification or an adjustment to a new material system can be realized with a few alterations to the digital model and printing parameters. This fast-evolving design-to-build cycle highlights the importance of continually expanding the range of materials available for AM.

Based on matrix materials, this chapter provides an overview of AM metal matrix composites (MMCs) and AM polymer matrix composites (PMCs), which often rival conventional and AM metals and alloys. Subsequent to this synopsis, the study's motivations and objectives are delineated.

1.1 Metal Matrix Composite (MMC)

Benefitted by improved strength, elastic modulus, and wear resistance, structural MMC is suitable for applications in industries including aerospace, automotive, space, defense, and sports. Lightweight structures can be made from matrix aluminum, titanium, and magnesium alloys reinforced by strong and hard reinforcements including Al_2O_3, SiC, TiC, B_4C particles as well as fibers and whiskers made of graphite, SiC, and Al_2O_3 (Seetharaman and Gupta, 2021, Kainer, 2006). Among all potential manufacturing processes, the most widely adopted ones were Laser Melting (LM) and Laser Deposition (LD), both requiring raw materials in their powder forms which are melted by the energy delivered in the form of laser (Seetharaman and Gupta, 2021).

In Figure 1.1, the apparatus of Selective Laser Melting (SLM) for manufacturing MMC is presented with major components. Similar to other AM methods, a 3D computer-aided design (CAD) model is necessary before starting the manufacturing process. Using a slicing software, the model can be sliced into 2D portfolios, which direct the laser beam to scan through a generated path on the surface of powders on the build platform. The energy will be transferred to the powders

at the scanned path, which is enough to melt the composite powders and allow them to fuse together upon cooling to form the defined 2D portfolio with a certain thickness. At this point, a layer of the product is complete, followed by the motion of the recoater which will deposit a new layer of unfused composite powders at the top after the Build platform lowers down. The laser then starts a new scan and melts the newly deposited composite powders according to a new portfolio, forcing the next fused layer to adhere to the previous one, increasing the thickness of the part and level of completion. After numerous repetitions, MMC can be manufactured into parts with different geometries as defined in the CAD model (Fereiduni et al., 2020). Despite its simple design, SLM can accommodate a wide range of metals, alloys, and MMCs, as long as they can be fed into the printer in powder form and melted under the heat supplied by the laser beam. However, excessive energy consumption and unstable melt pool which may cause significant shrinkage and geometric imperfections, in addition to substantial residual stresses, hinder the wide adoption of SLM in the production of MMCs (Seetharaman and Gupta, 2021).

Different from the SLM process, Laser Engineered Net Shaping (LENS) produces products by concurrent deposition of powders and laser illumination to form a melt pool on the substrate, as illustrated in Figure 1.2 below. The unique advantages of this manufacturing method include the ability to deposit on any selected substrate, which enables the deposited material to either join materials together or serve as a repair material for metal structures. However, its limitations include design constraints regarding building overhanging structures, requiring great surface finish, and the need to consider the effect of residual stress on the strength of the manufactured structure (Seetharaman and Gupta, 2021).

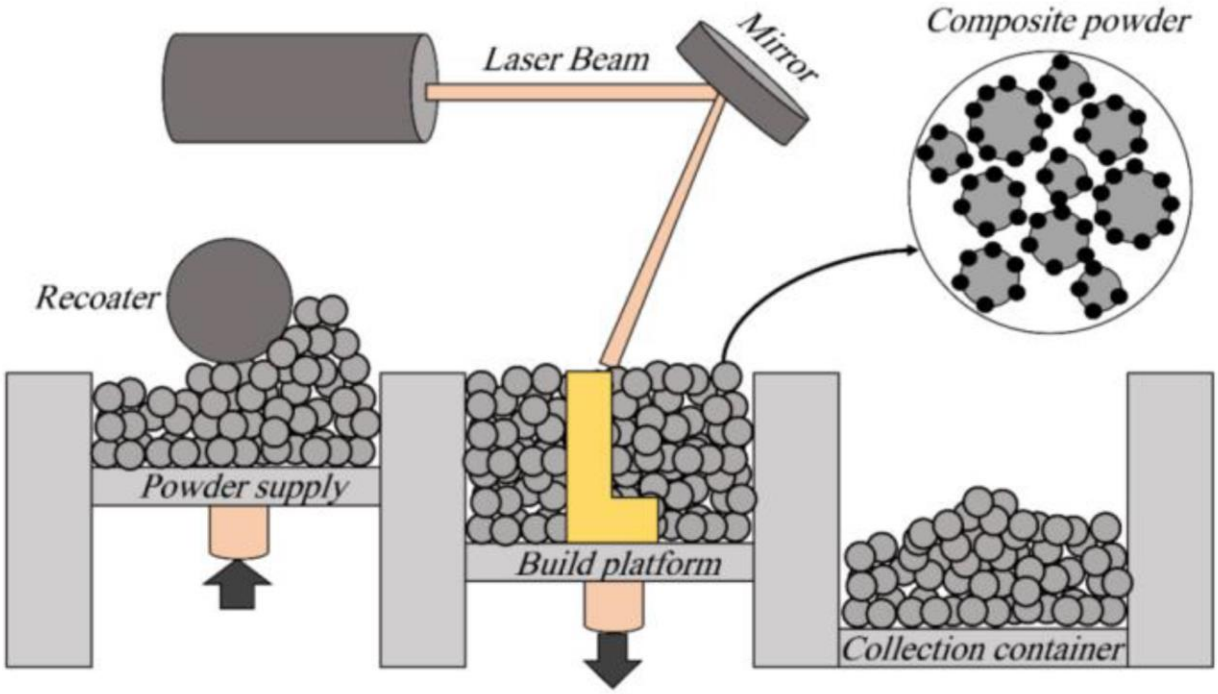

Figure 1.1. Schematic diagram illustrating the SLM manufacturing method when used to fabricate MMC. (Adapted from Fereiduni et al., 2020)

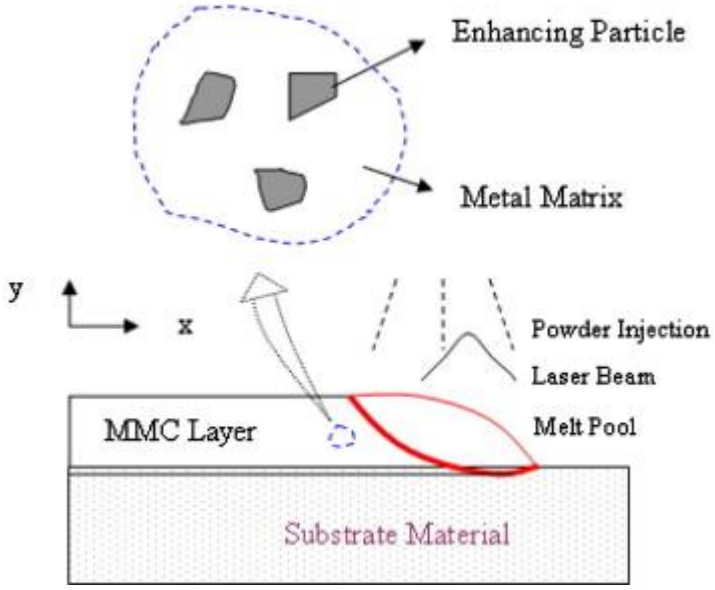

Figure 1.2. Schematic diagram illustrating the LENS manufacturing method and instantaneous microstructure of the deposited layer. (Adapted from Wen and Shin, 2011)

1.2 Polymeric Matrix Composite (PMC)

Similar to MMC, PMCs are often composed of distinguishable reinforcement and matrix phases. The reinforcement phase of PMCs is mostly short or continuous high-performance fibers, including carbon fibers, glass fibers, aramid fibers, and UHMWPE fibers. The matrix phase, as can be seen from the name of PMC, is composed of polymers that can be labeled as thermosetting or thermoplastic. This discrepancy in their behaviors upon elevated temperature caused different processing requirements and thus manufacturing methods for fabricating the derivative composites.

Short fibers are used as the reinforcement in PMC for a variety of reasons, including their accessible and low-cost nature, and compatibility with most existing polymer AM technologies. Short fibers can be divided into 2 groups based on their aspect ratios, such that milled fibers usually have lengths of hundreds of micrometers, and chopped fibers usually have lengths of millimeters (van de Werken et al., 2020). It was of note that the maximum fiber volume fraction within PMCs is limited and dependent on the fiber alignment and aspect ratio, such that higher performance associated with higher fiber volume fractions can only be achieved with well-aligned long fibers, as opposed to chopped and randomly distributed fibers (Fu and Lauke, 1996). As a result, continuous fibers became a desirable reinforcement for improving the mechanical properties of PMCs.

By introducing different fibers as reinforcement into polymers, the resulting structural PMCs can be benefitted in a variety of ways. Carbon fibers are often chosen due to their high specific strength and specific stiffness for making lightweight, strong, and stiff structures for aerospace applications. Glass fibers are typically chosen because of their cost-effectiveness with reasonable strength and stiffness, suitable for making large wind turbine blades and boats. Aramid fibers possess high specific strength, toughness, and impact resistance, making them candidates

for protective gear or armor. Ultra-High Molecular Weight Polyethylene (UHMWPE) fibers also exhibited high specific strength and toughness, allowing them to be used in impact protection.

1.2.1 AM of thermoset PMC

AM of PMC with a thermoset matrix can be achieved by the Direct Write (DW) or by reactive extrusion AM, both achieving controlled solidification after the deposition of material has been completed onto the build platform, as shown in Figure 1.3 below (van de Werken et al., 2019).

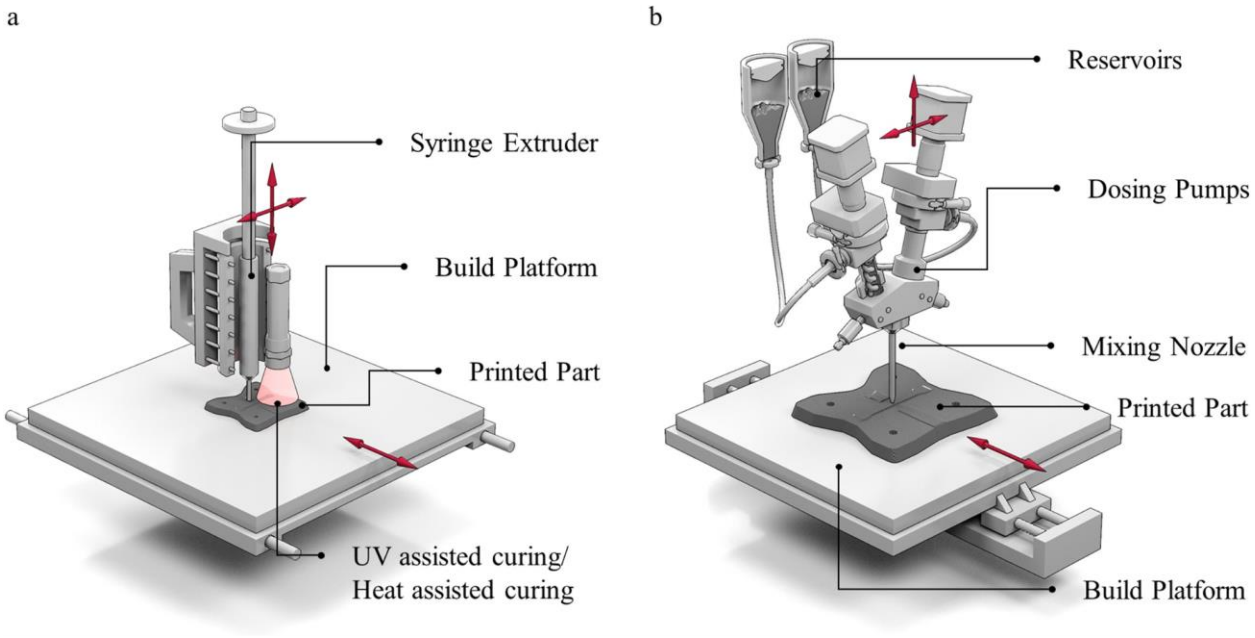

Figure 1.3. Schematic illustration with critical components of the apparatus showing a) the DW approach, and b) the reactive extrusion AM approach for additive manufacturing of thermoset PMC. (Adapted from van de Werken et al., 2019)

In the DW approach, shown in Figure 1.3 a), a thermoset PMC in its uncured form, including resin and catalyst (hardener) can be deposited in a controlled layer-by-layer fashion onto the build platform. The curing can happen in situ by an attached UV light or laser source, or subsequently after the deposition, if the viscosity was tuned and the deposited material was able

to maintain its shape without distortion (van de Werken et al., 2019). The delayed curing can be achieved via UV radiation or thermal exposure (Saito et al., 2019, Pierson et al., 2019).

In the reactive extrusion AM approach, the reactive resin and appropriate catalyst were fed through the mixing nozzle from two metering systems in a controlled manner to guarantee the thoroughness of mixing before being deposited (Rios et al., 2018). Upon deposition at a high rate, the resin cures exothermically under control.

With the stereolithography method, Sano et al. successfully printed PMC with UV-cure epoxy resin reinforced with chopped and continuous glass fibers (Sano et al., 2018). The process schematic is shown below to show the uniqueness of this method: a laser is directed to selectively solidify resin in predetermined regions within the tank which also contained pre-placed chopped and continuous glass fibers, after a layer of solidification was achieved, the structure was pulled upwards and allow for the liquid resin to fill the next layer.

Similar to the SLM presented above for MMC, Selective Laser Sintering (SLS) uses a laser to fuse PMC powders along a predetermined path in the top layer of the building chamber. The difference exists for the adjustable fusing temperature: for SLS, the goal is not to completely melt powders to create a melt pool and let it solidify to create a solid structure upon cooling, instead, the temperature is programmed to be slightly lower than the melting point of the powders such that they can be sintered together to form a shape. Yan et al., conducted research with SLS to manufacture carbon fiber/polyamide-12 composites and achieved improved flexural strength and modulus (Yan et al., 2011).

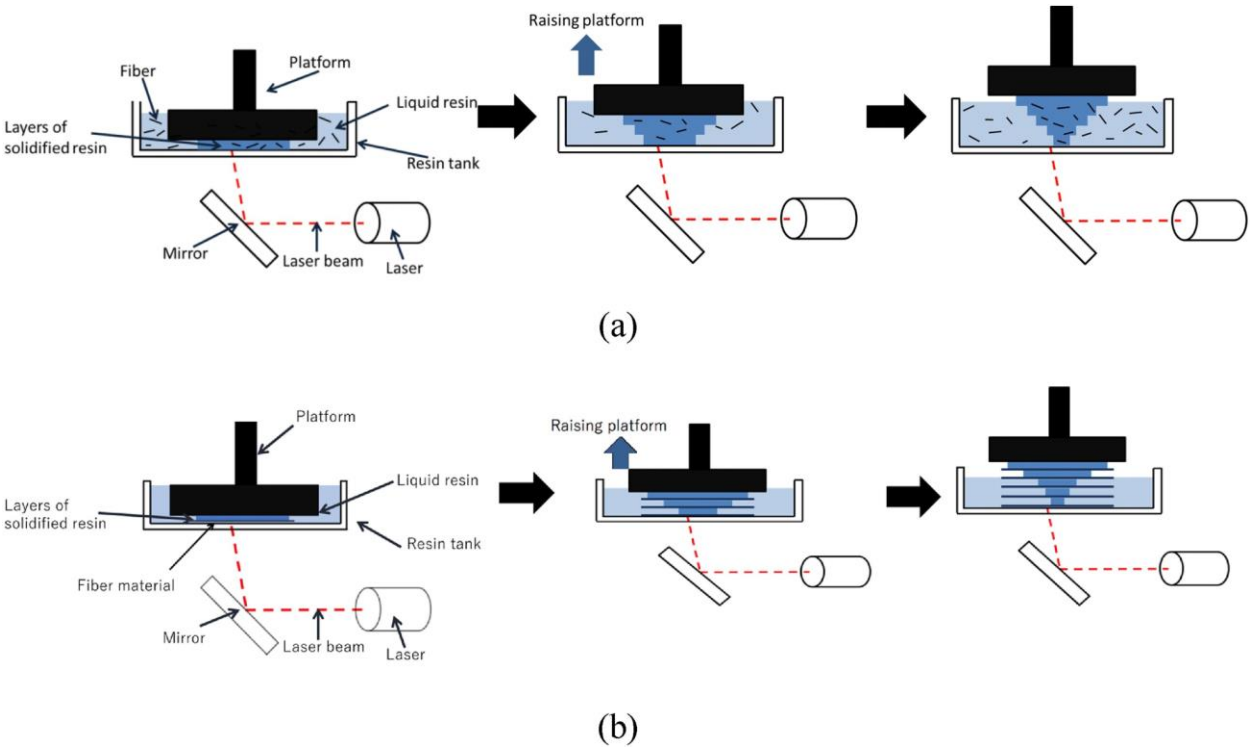

Figure 1.4. Process and apparatus schematic showing thermoset UV-curable PMC reinforced by chopped and continuous glass fibers. (Adapted from Sano et al., 2018)

1.2.2 AM of thermoplastic PMC

Depending on different physical forms of raw materials, most AM techniques regarding thermoplastic PMCs can be categorized into 2 kinds: differing from laser powder bed fusion (LPBF) based on powders, material extrusion is based on filaments (Tian et al., 2022). LPBF operates based on the same principles and procedures as SLM, shown in Figure 1.1. Material extrusion, commonly referred to as Fused Deposition Modeling (FDM) or Fused Filament Fabrication (FFF), operates based on the controlled deposition and extrusion of molten thermoplastic PMC filament onto the build plate. The heat was supplied from the hot printer nozzle programmed to maintain a temperature above the melting point of the thermoplastic polymer. After one layer of material has been deposited according to the predefined path based on the sliced CAD

model, the build plate lowers, or the nozzle assembly rises, to leave space for the next layer. It has been widely known for its simplicity, abundance in terms of raw materials, cost-effectiveness, and minimal waste (Safari et al., 2022). Many thermoplastics are available as FDM filaments, including polylactic acid (PLA), acrylonitrile butadiene styrene (ABS), polypropylene (PP), polyether-ether-ketone (PEEK), and polyamides (PA). Based on this simple while versatile design of the manufacturing process and apparatus, numerous thermoplastic PMC filaments reinforced by short and continuous fibers were developed. However, as researchers found that continuous fibers can improve the properties of PMCs much more effectively compared to short fibers, various attempts have been made to integrate continuous fibers into thermoplastic matrix polymers by means of pre-printing impregnation (Hu et al., 2017), co-extrusion (Wickramasinghe et al., 2020, Zhang et al., 2021), dual-extrusion (Wickramasinghe et al., 2020), compaction roller (Ueda et al., 2020), and post-printing integration (Mori et al., 2014, Amza et al., 2019).

Although the most straightforward fiber-impregnation method, co-extrusion, as shown in Figure 1.6 (left) is known for its simple one-step approach for printing PMC with continuous fibers, impregnation of continuous fibers was employed to better preserve the embedded fibers by forming resin membrane on their surfaces, and guarantee complete wetting of the fibers by the resin. It was argued that during the FDM process, using the printer nozzle alone may not be able to provide enough wetting of the fibers due to insufficient pressure and a short contact period (Hu et al., 2017). To enhance the integration of continuous fibers within the thermoplastic matrix after the deposition, a compaction roller attached to the printer nozzle, as well as heat treatments were employed and proved effective (Mori et al., 2014, Amza et al., 2019).

Unique defects may arise from the FDM process as there exist 2 interfaces at different length scales at which detachment can occur. On the micrometer level, interfaces between the

carbon fibers and the matrix polymer may provide sites for pores, causing undesirable integration of fibers within the PMC. This issue is more concerning for PMCs reinforced by short fibers, as the fibers within have larger surface areas compared to the continuous forms (Hu et al., 2017). The porosity problem becomes more severe for filaments produced without enough matrix impregnation, as the space between fiber strands may not be filled by the matrix polymer (Hu et al., 2017). On the sub-millimeter level, the incomplete fusion between different deposited PMC lines may leave vacancies and significantly decrease the properties of the printed structure (Tekinalp et al., 2014). This so-called inner-bead and inter-bead porosity is shown below in Figure 1.8.

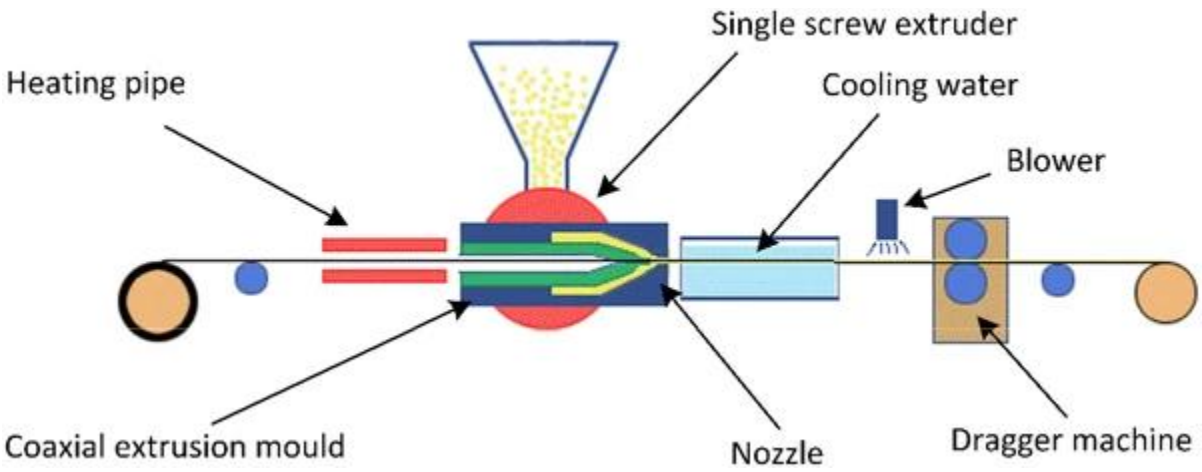

Figure 1.5. Coaxial impregnation of continuous carbon fiber to fabricate thermoplastic PMC filament for FDM. (Adapted from Hu et al., 2017)

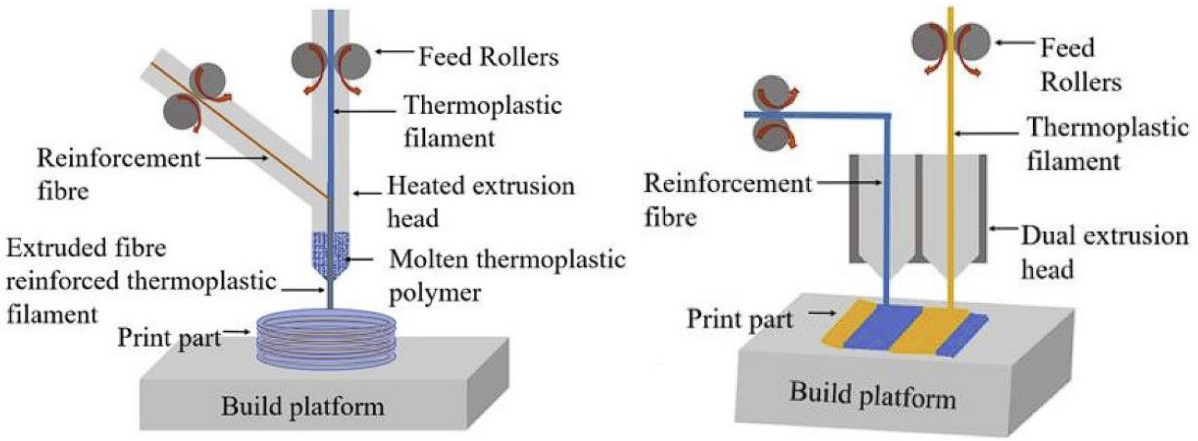

Figure 1.6. Schematics showing FDM of PMC via co-extrusion (left) and dual-extrusion (right). (Adapted from Wickramasinghe et al., 2020)

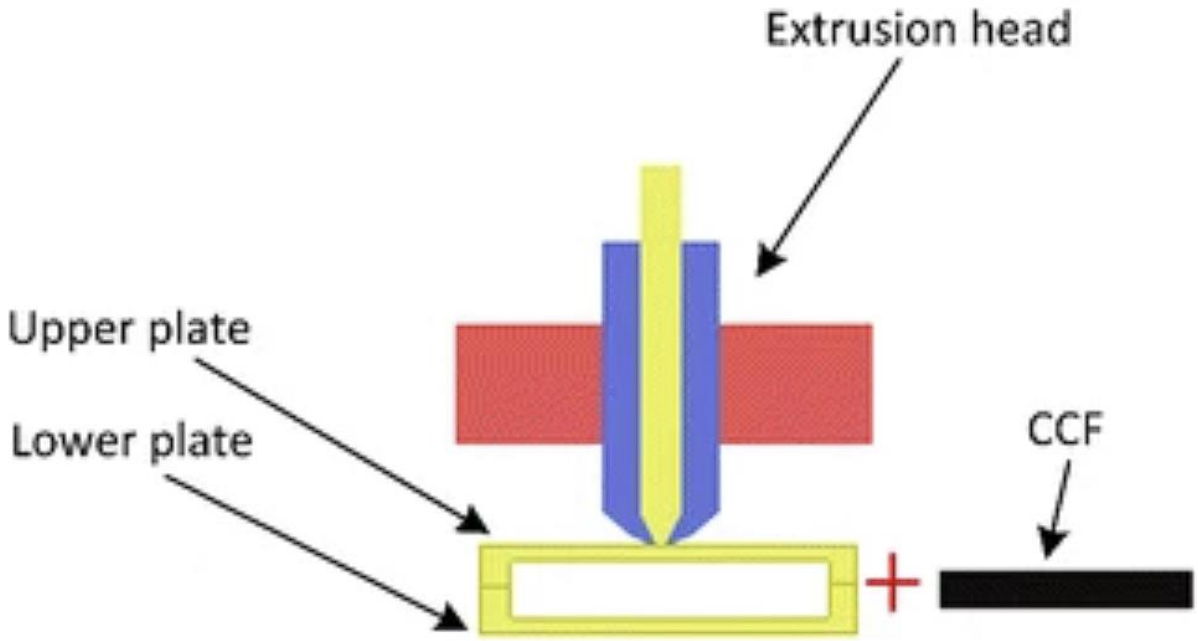

Figure 1.7. Schematic showing FDM of PMC via post-printing continuous carbon fiber (CCF) integration. (Adapted from Hu et al., 2017)

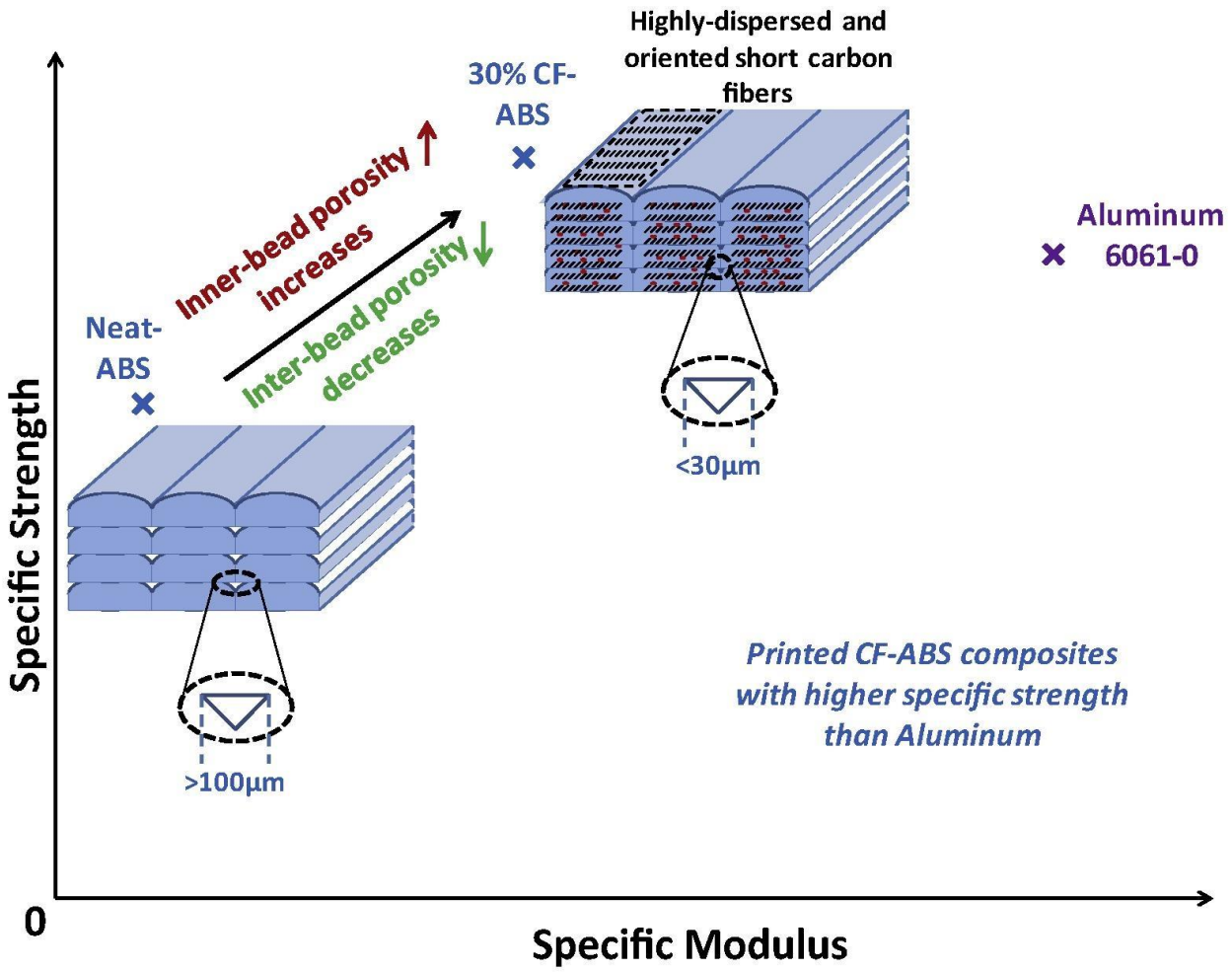

Figure 1.8. The porosity at different length scales for FDM PMC. (Adapted from Tekinalp et al., 2014)

While most of AM PMC literature focuses on the reinforcement of carbon fibers, the potential of UHMWPE fibers used as the reinforcement should not be omitted, despite some well-known challenges including low wettability and inertness, in addition to a low melting point, making them difficult to be physically and chemically integrated into AM PMC systems and allow efficient load transfer across the fiber-matrix interface (Chhetri and Bougherara, 2021). However, by carefully selecting appropriate thermoplastic polymers as the matrix, AM of UHMWPE can be achieved by FDM with extra processing steps. An exciting study presented the possibility of making UHMWPE-reinforced HDPE with FDM, as it had a considerable strength of 300.2 MPa

while demonstrating recyclability. More importantly, the integration of fiber within the PMC was achieved by complete impregnation and transcrystallization (Zhang et al., 2021). In another study, the introduction of manually placed UHMWPE fibers within the PLA matrix was proven effective in terms of improving the tensile properties. The integration of fibers was achieved by etching with chromic acid (Amza et al., 2019).

1.3 Objectives

As presented previously in this chapter, PMC reinforced by continuous UHMWPE fiber manufactured by AM has outstanding properties and a wide range of potential applications. The outstanding properties are a result of the fiber's intrinsic structure and properties. Notably, the fiber has great compatibility with AM because of its high toughness and flexibility, allowing unique designs requiring print paths with high curvature to be realized with lightweight and strong PMC. As a result, flexible impact-resistant protection can be achieved with an optimized structure design for load distribution and geometric compliance to the underlying objects.

Unique challenges are present and hinder the wide adoption of UHMWPE fiber as reinforcement of PMC, including its low melting point, poor interfacial adhesion to the matrix, and smooth surface. However, some other properties, including its low density, resistance to cryogenic conditions, durability against chemical attacks, and high electrical resistance, make these fibers suitable for applications in harsh environments. One can imagine a possible application of PMC reinforced by UHMWPE fiber as the protective layer of satellites and spaceships against impacts. Due to its low absorbance of a wide range of electromagnetic radiation, protecting the solar panels with these composites is also possible. The high toughness and flexibility can also be combined with the self-extinguishing property, which may be of interest when used as spacesuits and mine clearance suits.

In this study, a composite filament for FDM with high-performance continuous UHMWPE fiber tows was made and validated. The specific objectives are to:

1. Assess the feasibility of filament-making apparatus resembling the pultrusion process, as iterated from the previous attempts resembling co-extrusion;
2. Examine the microstructure of the developed composite AM filament before and after printing to identify fiber damage and defects within the composite;
3. Evaluate the mechanical properties of the developed filament before and after printing to identify influential processing factors;
4. Establish the processing-structure-property relationship of the composite and suggest potential applications;
5. Provide insights for further improvements.

Overall, the results and efforts presented in this document draw an important connection between the structure, processing methods, properties, and performance of a new composite filament suitable for FDM and provide new possibilities for designing and manufacturing next-generation high-performance composite structures.

Chapter 2 - Materials and Methods

2.1 Filaments

The composite material system produced and investigated in the form of filaments were composed of strands of UHMWPE yarn (SK99 dtex880, 0.975g/cm^3, Dyneema®, DSM, Greenville, North Carolina) embedded in polycaprolactone (PCL) matrix (molecular weight = 50,000, Material Sample Shop, Denmark), which is denoted as Dyneema/PCL here. Dyneema was chosen as the reinforcement in this study primarily because of its high strength and low density in addition to its superior durability when exposed to chemicals, moisture, and UV (Avient, 2023). However, this thermoplastic fiber has a relatively low melting point between 144℃ and 152℃ (FibrXL, 2020), which makes it susceptible to thermal damage during filament fabrication and printing processes and requires a matrix material that has a lower melting point. Considering this and the commercial availability, PCL was selected as the ideal matrix polymer, as its melting point is only 60℃ (Material Sample Shop, 2013). In preliminary filament-making experiments, a commercially available PCL filament (Facilan PCL 100, 1.1g/cm^3, molecular weight = 50,000, 3D4Makers B.V, The Netherlands) for AM was used accompanying Dyneema, denoted as Facilan.

2.2 Filament Fabrication

Developed based on the pultrusion method, as shown in Figure 2.1 for manufacturing polymer composites with a constant cross-section (Minchenkov et al., 2021) and a benchtop system for embedding carbon fiber in ABS matrix (Matsuzaki et al., 2018), an assembly was constructed as shown in Figure 2.2. A brass nozzle with an internal diameter of 0.8 mm was fixed at the exit point of the UHMWPE fiber tow in the aluminum tank to control the diameter of the produced filament by removing excess molten PCL. A thermocouple was installed at this nozzle

to monitor the exit temperature so that the hot plate could be adjusted to maintain it at 75℃. As the filament got pulled towards the Filabot spooler (Precision Filament Winder, FB00073, Vermont) at a constant rate of 0.25 cm/second, it was cooled by a fan to maintain a constant cross-sectional shape (Marquis et al., 2023). The volume fraction of the fiber in the filament was then calculated according to

$$V_{fiber} = \frac{A_{fiber}}{A_{nozzle}} = \frac{\frac{dtex}{\rho L}}{1/4\pi d^2} \quad (1)$$

where A_{fiber} and A_{nozzle} is the cross-sectional area of the fiber tow and nozzle, respectively, $dtex$, is the linear density of the fiber tow in grams/10,000 m, ρ is the density of the fiber tow, L is 10,000 m that is intrinsically associated with the unit dtex, and d is the internal diameter of the nozzle. V_{fiber} obtained this way is 18%, representing the theoretical minimum value assuming negligible shrinkage of the filament induced by cooling and minimal fiber waviness. A_{fiber} and A_{nozzle} are 0.0903 mm^2 and 0.502 mm^2, respectively. Depending on the intentional fiber distribution manipulation by separating fibers while it passes through the PCL bath, 2 kinds of filaments were produced and used for FDM feedstock materials, denoted as WDF (with dispersed fibers) and WODF (without dispersed fibers).

2.3 Sample Preparation by FDM

FDM of the filaments was realized with a Prusa Model I3 MK3S printer (Prague, Czech Republic) modified in the following fashion: an independent temperature controller (OMRON, E5CB, Kyoto, Japan) was attached to the heater block which was powered by a 24V DC, 15 Amp switch power supply. With an attached Type K thermocouple, a constant temperature was maintained at 120℃ during the FDM process. Filaments were extruded through a brass nozzle

with an internal diameter of 1.2 mm at a rate of 100mm/min on a spring steel print bed (FYSETC, Guangdong, China). It was noteworthy that the printer nozzle had a slightly larger diameter compared to the exit nozzle mounted at the exit of the PCL bath, as the former needed to accommodate possible geometric imperfections of the filament after it was pultruded through the latter. To promote adhesion between the initial section of the printed filament and the print bed, the filament was first inserted into the printer through the nozzle before heating up and the initial section (~5mm) of the filament was mechanically pressed down onto the print bed using a tweezer. To prepare linear printed samples with a required length to accommodate the special fixtures as shown in Figure 2.3, two printers of the same type were placed facing each other and operated in tandem, with a steel sheet replacing both print beds. The printers were programmed in a way such that when the primary motor assembly reached its maximum operable limit, the secondary motor assembly in the other printer would immediately push the steel plate until the desired length was deposited, at which point the filament was cut using specialized scissors and removed from the steel sheet. For assessing the printability of filaments when creating more complicated geometries, the nozzle was programmed to slightly lower at the turns in order to ensure the predeposited filament was secured into place instead of being dragged away (Zhang et al., 2022). At these curved portions in the tool path, a slower printing speed of 10mm/minute was also necessary to produce the desired geometry, so that the PCL can cool down sufficiently and allow the embedded compliant fibers to get fixed before turning (Marquis et al., 2023).

Of note, the preliminary Dyneema/PCL FDM fabrication was set up as inspired by the co-extrusion FDM method, as illustrated in Figure 1.6 (left). The Dyneema fiber tow and Facilan were fed into the printer and through a 2 mm printer nozzle before the nozzle was set to maintain 120℃. To allow continuous deposition, manual pulling was required, as the feed rollers inside the printer

were not able to provide enough clamping force to prevent the Dyneema fibers in contact from slipping, due to the low-friction surface of these fibers. When excessive clamping force was applied, due to the low flexural stiffness of the fibers, they would bend in the transverse direction, and then slip off the surface of the rollers. Therefore, continuing extrusion based on was considered impossible in this way. In rare cases when short sections of PCL/Facilan successfully exited the hot printer nozzle, the impregnation of Facilan into the fiber tows was unacceptable and left most fibers exposed and not coated, as shown in Figure 2.4. Because of the undesirable structure observed and the fact that by co-extrusion, Dyneema fiber tows passing through the nozzle would be in direct contact with the hot nozzle which eliminated the fiber's stiffness, and cause discontinued printing as the fibers would no longer be able to transfer the pulling force, co-extrusion experiments were no longer conducted and eventually replaced by the PCL bath approach which allowed for continuous production.

2.4 Microstructure analysis

The microstructure of filaments in different conditions was examined using an optical microscope (Model BX51M, Olympus Corporation, Tokyo, Japan) with an attached digital camera (1024 × 768 resolution). In order to observe the cross-section of the filaments, small sections were cut with specialized scissors and mounted in the Epofix HQ Resin/Hardener mixture. After the resin hardened, a successive series of polishing pads from #400 grit to #1200 grit was used to reveal microstructural features.

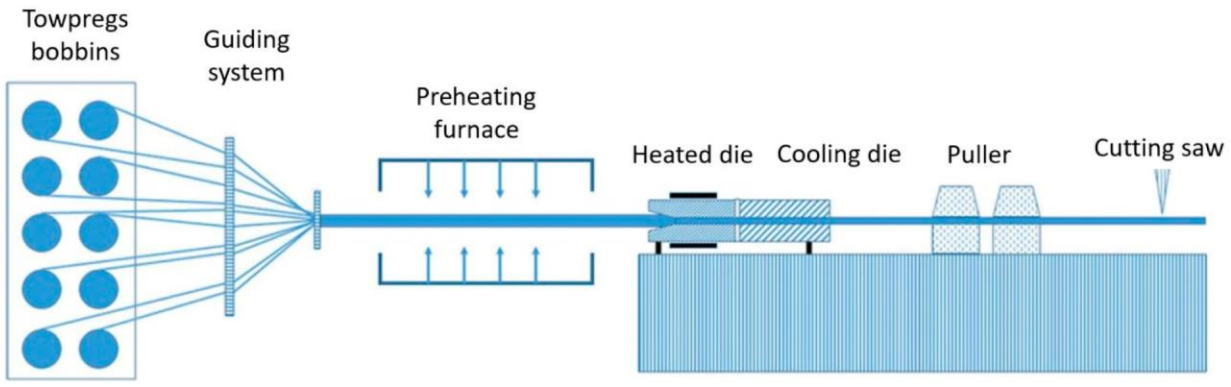

Figure 2.1. Schematic diagram of nonreactive pultrusion manufacturing process. (Adapted from Minchenkov et al., 2021)

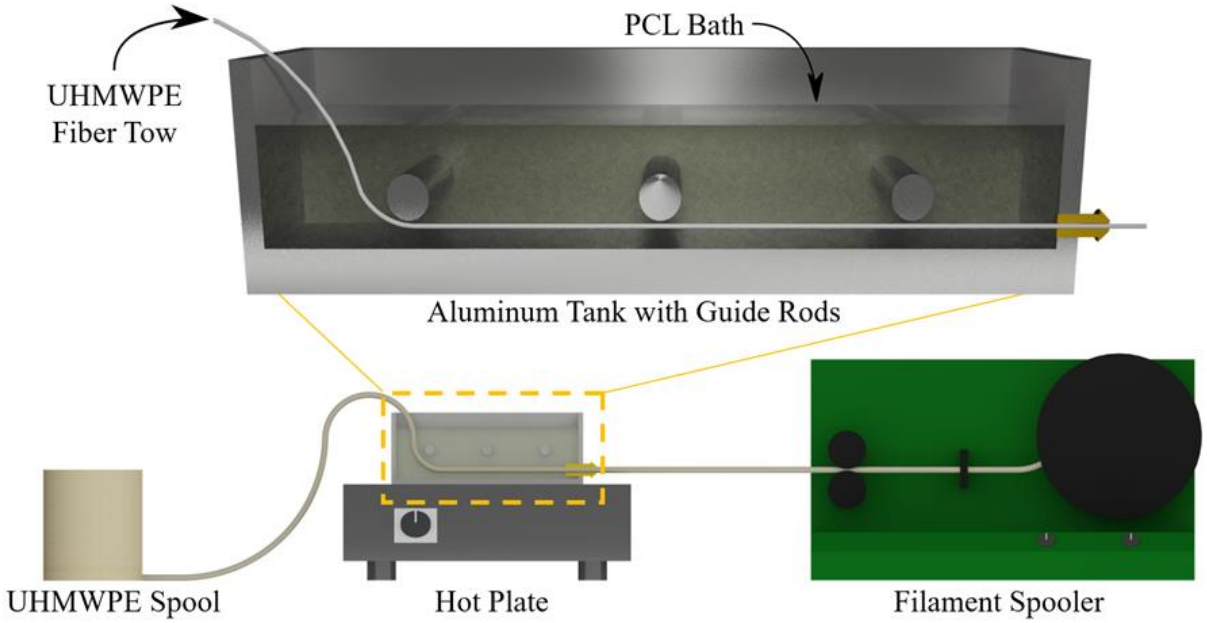

Figure 2.2. Filament manufacturing assembly with enlarged aluminum tank setup showing UHMWPE fiber tow in PCL bath. (Adapted from Maquis et al., 2023)

2.5 Mechanical Analysis

Uniaxial tension tests were performed on the as-received UHMWPE fiber tows and the Dyneema/PCL composite filaments in different conditions using an Instron E1000 load frame (Instron Corporation, E1000, Morwood, MA, USA) with special fixtures as shown in Figure 2.3.

15 samples were prepared for each type of filaments. Fixtures were designed to prevent slipping between the samples and the fixtures or undesired failures due to excessive clamping force or friction outside the gauge section. To mount the filaments onto the fixture, it was necessary to wrap the filament around the top and bottom circular axles once to prevent concentrated load at A and B which may cause undesired failures outside the gauge section CD. The gauge section CD was designed to align the loading axis of the instrument and had a length of 145 mm when set up properly. The length of one sample tested in this manner was 700 mm. C-clamps were used with metal backing plates and sandpaper to provide enough clamping force while protecting the fixture surface from compressive damage. The grips were additively manufactured using Markforged Onyx material with 55% infill.

At a loading rate of 5 mm/minute in the displacement control mode, these tests were able to generate load-displacement data which can be then evaluated for understanding material-specific tensile responses according to

$$\varepsilon = \frac{\Delta L}{L_0} \tag{2}$$

$$\sigma = \frac{F}{A} \tag{3}$$

where ε is the engineering strain, ΔL is the displacement measured by the instrument, L_0 is the gauge length, σ is the engineering stress, F is the load, and A is the cross-sectional area of the sample. Based on Equations 2 and 3, the ultimate tensile stress at failure, σ_f and the corresponding tensile strain, ε_f, are reached at the point when F reaches the maximum. Tensile toughness can then be calculated according to

$$U_T = \int_0^{\varepsilon_f} \sigma \, d\varepsilon \tag{4}$$

where U_T is the toughness of the material, or energy of mechanical deformation per unit volume prior to fracture. Numerical integration by trapezoidal rule was used in this paper to calculate the value of U_T.

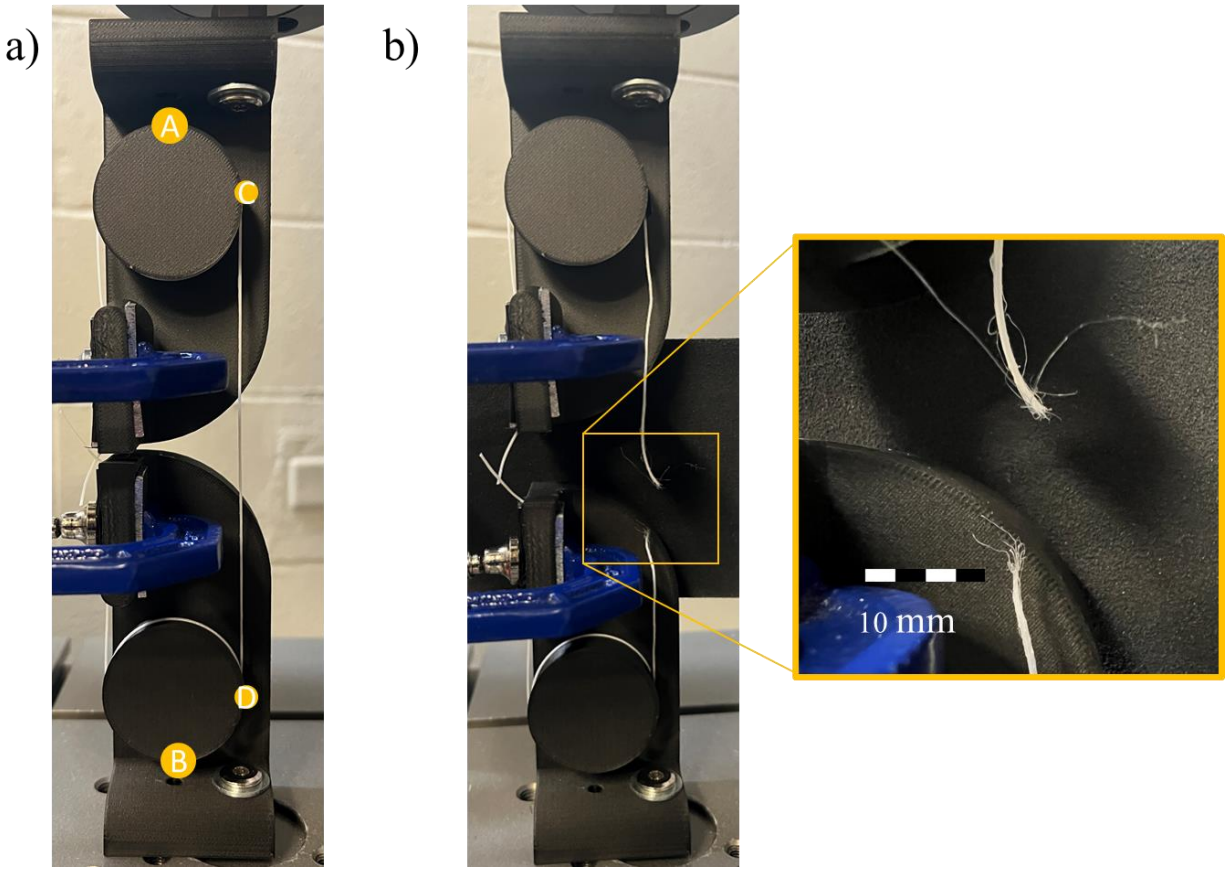

Figure 2.3. Tensile testing of a filament using special fixtures. a) filament undergoing uniaxial tensile testing while under load. b) Filament after failure in gauge section.

To quantitatively estimate the fiber degradation in terms of its strength in different samples, apparent fiber strength (AFS), was calculated by applying the Rule of Mixing (ROM):

$$AFS = \frac{\sigma_{f,composite} - \sigma_{f,matrix}(1 - V_{fiber})}{V_{fiber}} \tag{5}$$

which can be used for filaments WDF and WODF before and after printing, providing that the $\sigma_{f,matrix}$ is 16.9 MPa (Rosa et al., 2004).

The reliability of the filaments in different conditions as well as the as-received UHMWPE fiber tows were evaluated by two-parameter Weibull analysis with their σ_f according to

$$P(\sigma) = 1 - exp(-(\frac{\sigma}{\sigma_0})^m) \quad (6)$$

where $P(\sigma)$ is the probability of failure at the stress of σ, σ_0 is the characteristic strength, and m is the Weibull modulus. The probability of failure was defined by an estimator function such that

$$P_f\ (i) = \frac{i - 0.5}{N} \quad (7)$$

where $P_f\ (i)$ is the probability of failure for the ith sample in the ranking of σ_f from the smallest to the greatest, and N is the total sample count in the group. Therefore, solving for P_f and setting $ln(ln(1/(1 - P_f))) = 0$ can give σ_0 and a corresponding $P_f \approx 63.2\%$.

Two-way Analysis of Variance (ANOVA) was employed to examine the effectiveness of the chosen independent variables related to filament conditions and configurations on their properties. Namely, how fiber dispersion (WDF or WODF) and printing (filament and printed) exert influence on σ_f.

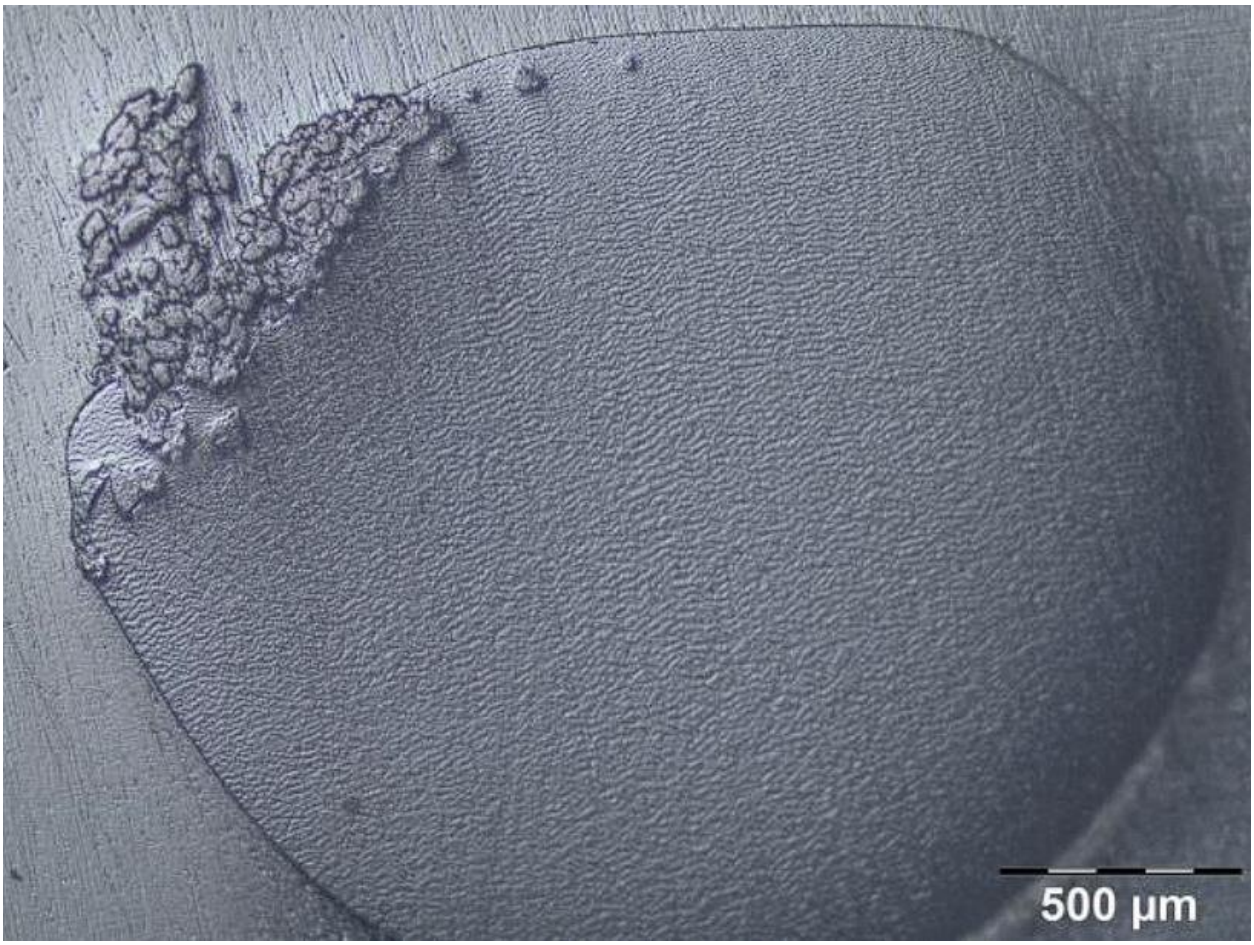

Figure 2.4. Cross-section of Dyneema/Facilan composite produced by co-extrusion.

Chapter 3 - Results

3.1 Microstructure of Dyneema/PCL composites

With optical microscopy, the cross-sections of different Dyneema/PCL samples were observed for their microstructural features and defects. Generally, for single-path filaments and printed samples as presented in Figures 3.1 and 3.2, few voids were found, indicating great compatibility of Dyneema fibers and the PCL matrix under appropriate processing conditions. Micrographs at higher magnifications, such as those shown in Figure 3.1 a) and Figure 3.2, showed that sufficient PCL coating was present around the Dyneemal fiber bundles, in contrast to the more limited coating of individual fibers when they were surrounded by others in closely-packed fiber bundles. As the fiber volume fraction (V_{fiber}) was designed to be at a low value for these shown samples at 2.9%, most of the cross-section of Dyneema/PCL composites consisted of pure PCL without Dyneema reinforcement. The difference in fiber dispersion configuration was clearly illustrated by comparing Figure 3.1 a) with b), as dispersed fibers in Filament WDF samples formed distinguishable small bundles each containing tens of fibers, more evenly distributed around the center of the cross-section, and undispersed fibers formed a single bundle group mostly to the right side of the center.

Uneven distribution of fibers was also observed for composites in their printed condition, as shown in Figure 3.2, even the corresponding filament contained distributed fibers. The fibers spread in the region close to the central upper surface of the deposited single-path composite layer, with some of them directly exposed to the environment with little PCL coated as the protection layer.

The cross-section of a two-layer printed bar shown in Figure 3.3 revealed additional problems compared to composites in their filament and printed forms, namely the large voids at

layer interfaces, and poor geometric accuracy around the periphery of the cross-section. The poor geometric accuracy can be observed in normal-scale photos, such as shown in Figure 3.4, in the form of grooves between adjacent print paths and layer mismatches around the periphery of the disk.

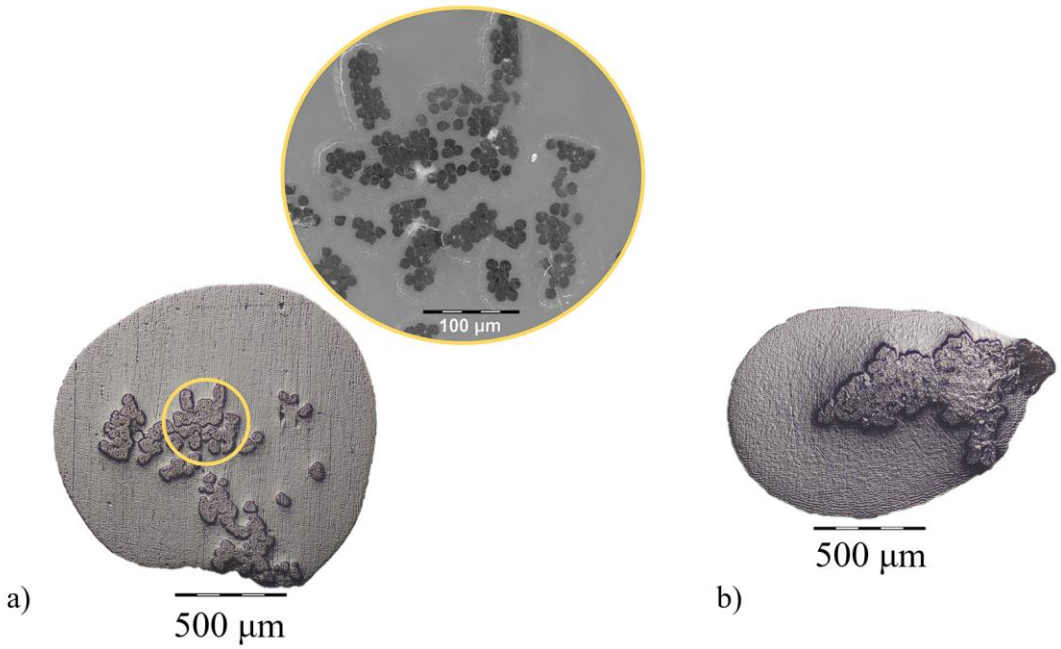

Figure 3.1. Micrographs of the a) Filament WDF composite and b) Filament WODF composite, both pultruded through a 2.0 mm tank nozzle. Magnified regions display darkfield images of fibers.

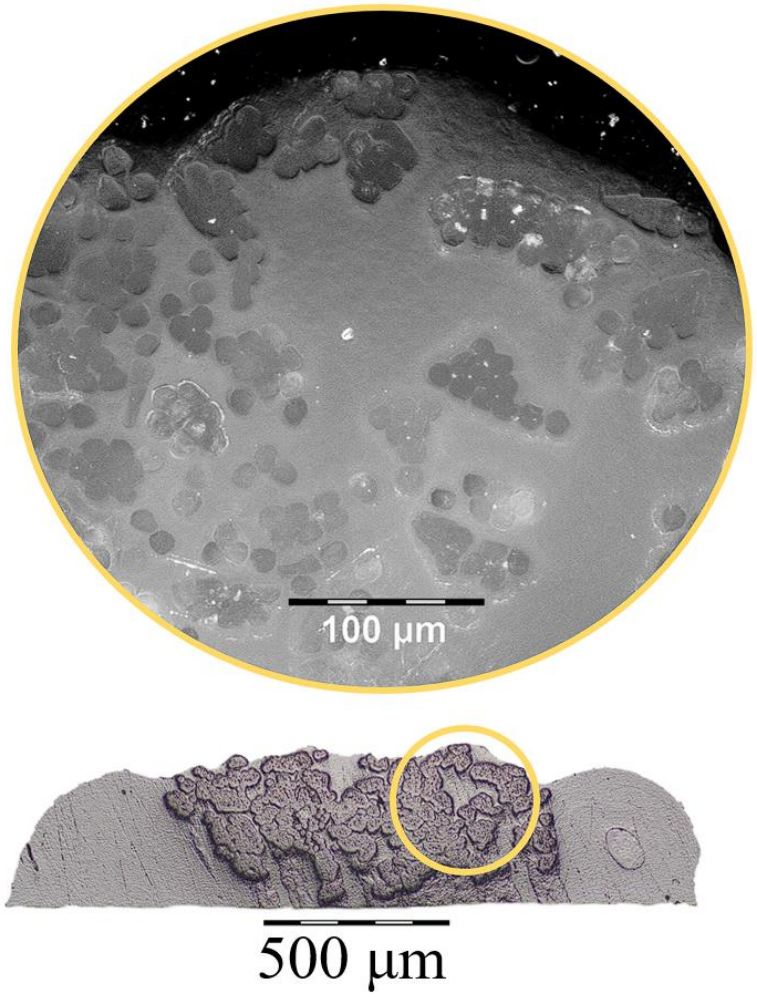

Figure 3.2 Micrographs of the Printed WDF composite pultruded from a 2 mm tank nozzle and printed through a 1.2 mm nozzle. Magnified regions display darkfield images of fibers.

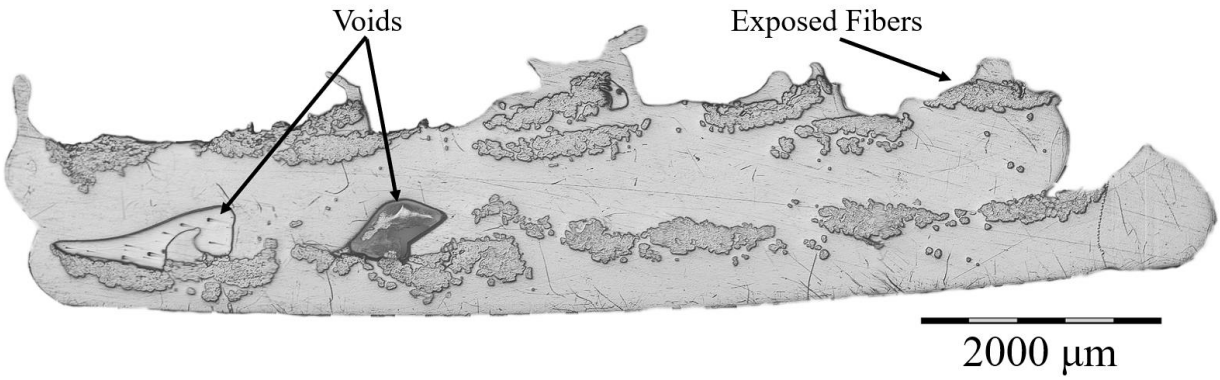

Figure 3.3 2-layer print of UHMWPE reinforced PCL composite with 5 print paths on each layer

Figure 3.4. A printed Dyneema/PCL composite disk with a bouligand structure

3.2 Tensile Properties

In both Figures 3.5 and 3.6, wave-like features were evident near the fracture point of the samples, shown as local fluctuations in the stress-strain plots. This characteristic was accompanied by an audible cracking sound during testing, indicating that a fracture occurred within the fibers of the samples. These findings suggest that the inherent structural integrity of the filaments experienced some level of compromise under the applied stress conditions.

Figure 3.5, presenting stress-strain relationships of Dyneema samples under uniaxial tensile loading, displays two distinct regions. The initial region is characterized by a relatively low slope, extending up to approximately 200-300 MPa when extensive preloading was not present. This is followed by a range up to the fracture which Dyneema demonstrates a steep stress-strain curve, indicating its high degree of structural resilience and resistance to deformation. These

behaviors, in addition to the relatively low values of strain at fracture around 2%, demonstrated that the Dyneema fiber is a brittle material with little yielding, in other words, possesses relatively linear stress-strain correlations.

Figure 3.6 encompasses four different composite types: Filament WDF, Filament WODF, Printed WDF, and Printed WODF. The stress-strain relationships for these samples are more complex, consisting of three regions. The first region, similarly to Dyneema, is characterized by a low slope and continues up to around 100 MPa. The second region can be distinguished by a high-slope phase. For filament samples, this phase extends up to a strain of about 2%, where Dyneema approaches its fracture point. This high slope indicates an increase in the composite's resistance to deformation. For printed samples as shown in Figure 3.6 c) and d), this high slope phase is more limited, typically between 1.5% to 2% strain. The third region observed in Figure 3.6 displays a return to a low-slope trend compared to the previous phase. Of note, Printed WDF samples exhibited little strain returning, and most of them fractured at strain values of around 2% close to those of Dyneema fiber tows, as shown in Figure 3.5.

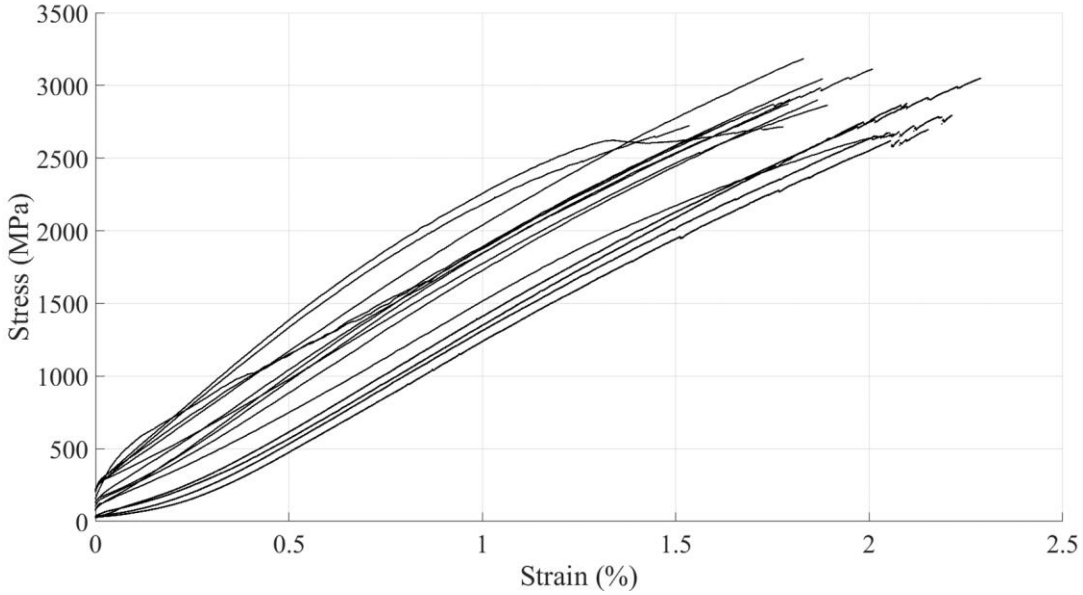

Figure 3.5. Stress-Strain relationships of Dyneema fiber tows

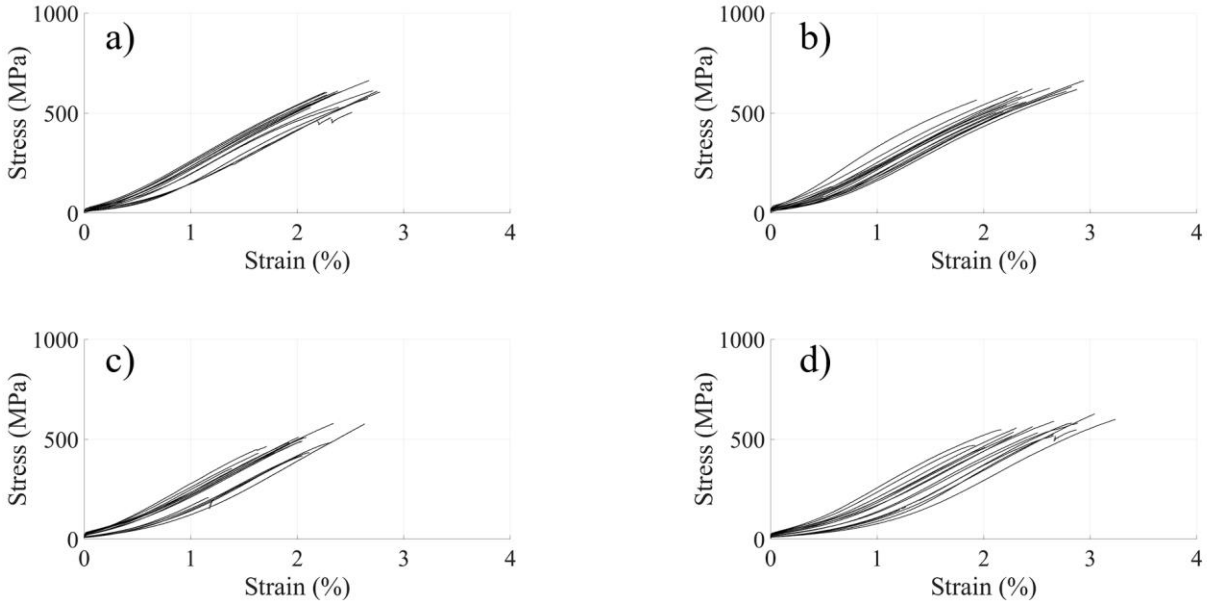

Figure 3.6. Stress-strain curves for filament and printed samples with V_{fiber} = 18%. a) Filament WDF, b) Filament WO DF, c) Printed WDF, d) Printed WODF.

Figure 3.7 provides a comprehensive comparison of the stress and strain at fracture of all samples subjected to tensile tests. The corresponding values are presented as the average (shown by the height of bars) ± standard deviation (shown by the error bars at the top) to account for the variations across samples.

Dyneema demonstrated the highest strength among the tested materials, with a value of 2876±160 MPa at a strain at failure value of 1.92±0.21%. The Filament WDF and Filament WODF samples showed similar strength values, 588±41 MPa and 586±43 MPa, respectively. The strain at fracture was also similar for these two filament types, with Filament WDF at 2.46±0.21% and Filament WODF at 2.45±0.29%. On the other hand, both Printed WDF and Printed WODF exhibited decreased strengths in comparison to their filament forms, with values of 474±62 MPa and 548±46 MPa, respectively. The strain at fracture for these printed samples were 2.02±0.30% for Printed WDF and 2.54±0.38% for Printed WODF. This decrease in strength after printing could

be attributed to the degradation of filaments during the printing process. Despite the reduction, both printed samples displayed reasonably high strength retention and promising mechanical performance.

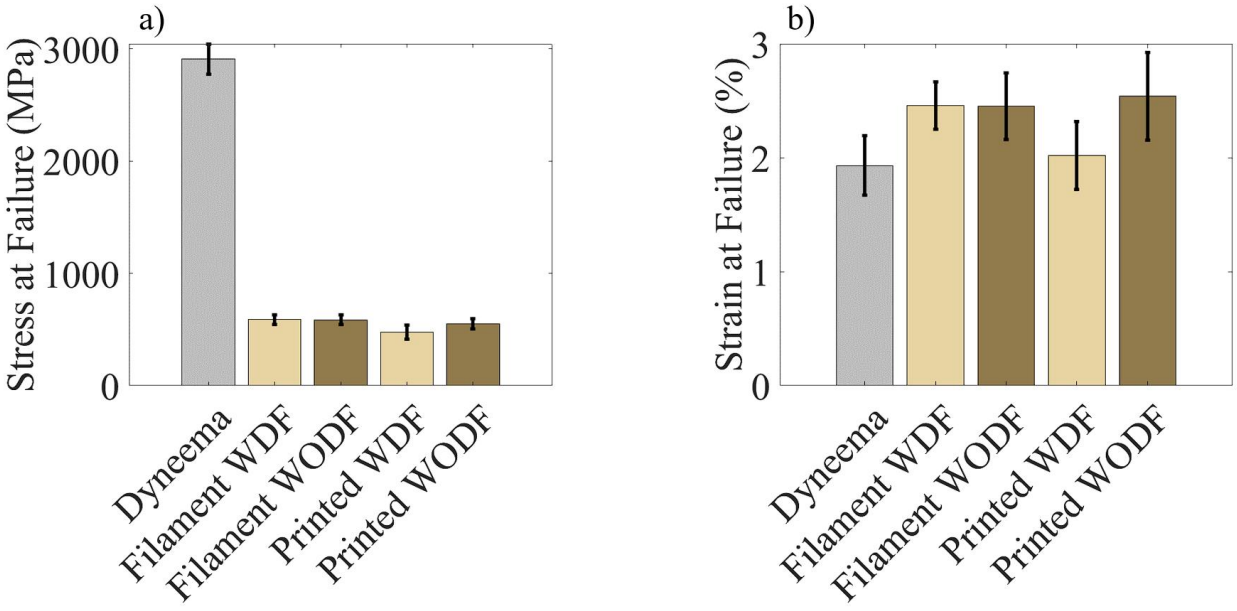

Figure 3.7. Mechanical properties of the samples before and after printing. a) Stress at failure, and b) Strain at failure.

3.2.1 Toughness

In Figure 3.8, results generated from the toughness analysis of various samples were presented using numerical integration based on their stress-strain data. The Dyneema fiber tows had a toughness of 30.8 ± 3.0 MJ/m^3. In comparison, both kinds of filaments had considerably lower toughness values of 6.9 ± 0.86 MJ/m^3 corresponding to Filament WDF samples and a slightly higher value of 7.1 ± 1.2 MJ/m^3 for Filament WODF samples. After undergoing printing, both the Printed WDF and Printed WODF samples exhibited a reduction in toughness, with values of 4.5 ± 1.1 MJ/m^3 and 6.2 ± 1.1 MJ/m^3, respectively. This observed trend parallels the patterns previously identified in data and their relationships as demonstrated in stress-strain curvess as shown in Figures 3.5, 3.6, and 3.7.

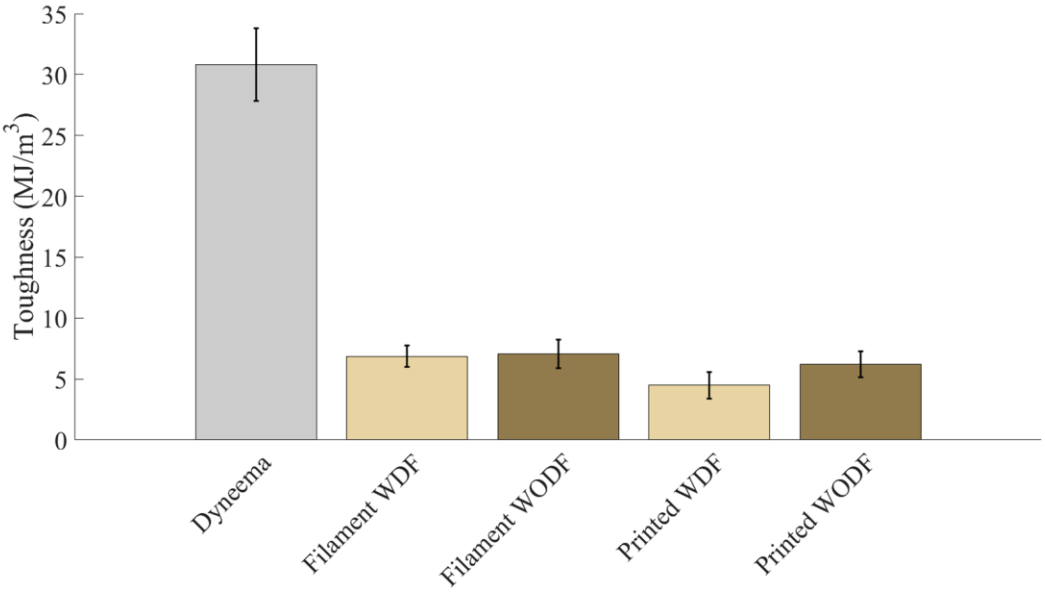

Figure 3.8. Toughness of the samples before and after printing.

3.2.2 Apparent Fiber Strength (AFS)

To quantify the retention of fibers, the Apparent Fiber Strength (AFS) for all kinds of composite samples investigated was placed in adjacent to the strength of as-received Dyneema fiber tows in Figure 3.9. The data, presented as average values accompanied by standard deviation, yielded several observations. Interestingly, Dyneema fibers in Filament composites exhibited the highest strength, 3187 ± 225 MPa for fibers if they were in Filament WDF, and 3176 ± 237 MPa for fibers in Filament WODF. Both values are considerably higher than 2876 ± 160 MPa for as-received Dyneema fiber tows and their printed forms: 2558 ± 346 MPa for Printed WDF and 2967 ± 254 MPa for Printed WODF. From this analysis, it was deduced that, excluding the Printed WDF samples, the encasement of Dyneema fiber tows within the PCL matrix enhanced their load-bearing capability. Conversely, fiber exposure, as depicted in Figure 3.2, severely hinders this desirable protective effect and makes the fiber susceptible to environmental damage, namely the excessive heat conducted from the printer nozzle.

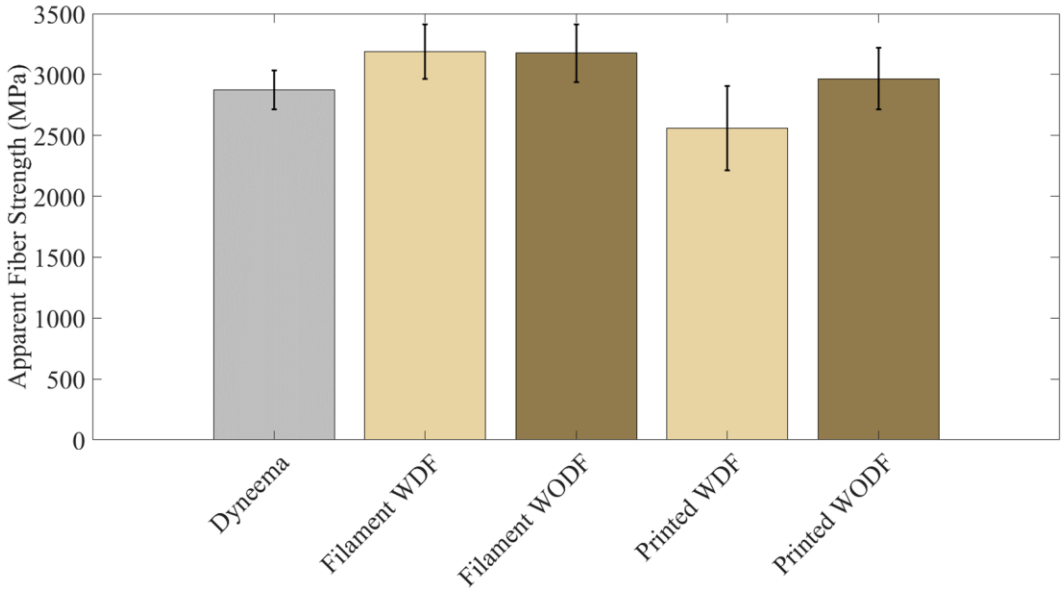

Figure 3.9. Apparent fiber strength (AFS) of the samples before and after printing

3.2.3 Weibull analysis

Evaluation of the reliability of as-received Dyneema fiber tows and their composites were conducted in the form of Weibull analysis, as visualized in Figure 3.10. It can be seen that the Weibull modulus of each type of material often differs, as the slopes of fitted lines are often distinguishable from each other in the Weibull plot. Among all sample types, as-received Dyneema fibers possessed the highest m and characteristic strength of 20.7 and 2950 MPa, respectively. Filament WDF and Filament WODF had slightly lower but very similar m of 16.6 and 16.3, with characteristic strengths of 606 MPa and 604 MPa, respectively. Printed WDF suffered poor reliability as its m was only 9.0 with a σ_0 of 500 MPa, both were the lowest values among all types of samples examined. In contrast, after undergoing the printing process, Printed WODF demonstrated better reliability with an m value of 14.3 and σ_0 of 568 MPa.

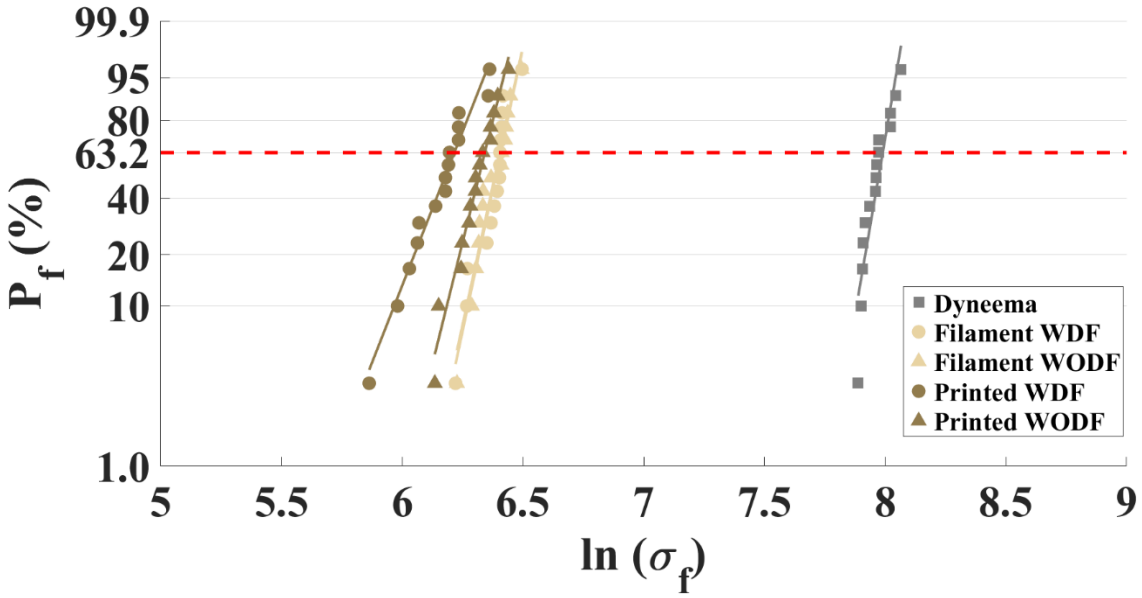

Figure 3.10. Weibull plots for filaments prior to printing and in the printed state compared to the unprocessed Dyneema fiber tows. The red dashed line corresponds $P_f \approx 63.2\%$, where $ln(ln(1/(1-P_f))) = 0$, and intersects fitted lines at $ln(\sigma_0)$.

3.2.4 ANOVA

In this study, two factors were included in the experimental design and exerted statistically significant influence on the strength of Dyneema/PCL composites, namely the fiber dispersion configuration, denoted as WDF and WODF, and whether the composites underwent printing after pultruded into the filament form, denoted as Filament and Printed. Two-way ANOVA examination with 15 replications proved that both factors were statistically important, with P values of 0.00600 corresponding to the fiber dispersion configuration factor, 1.43E-7 corresponding to the printing condition factor, and 0.00389 corresponding to their interaction parameter, all much smaller than 0.05, which is a common benchmark for examining the statistical significance of a chosen independent variable.

Chapter 4 - Discussion

For structural applications, the strength of composites is often a critical factor to be considered. To contextualize the notable achieved properties of the investigated Dyneema/PCL system, a relatively comprehensive comparison relating strength to V_{fiber} of different commercially available and laboratory-scale fiber-reinforced composites is presented below in Figure 4.1.

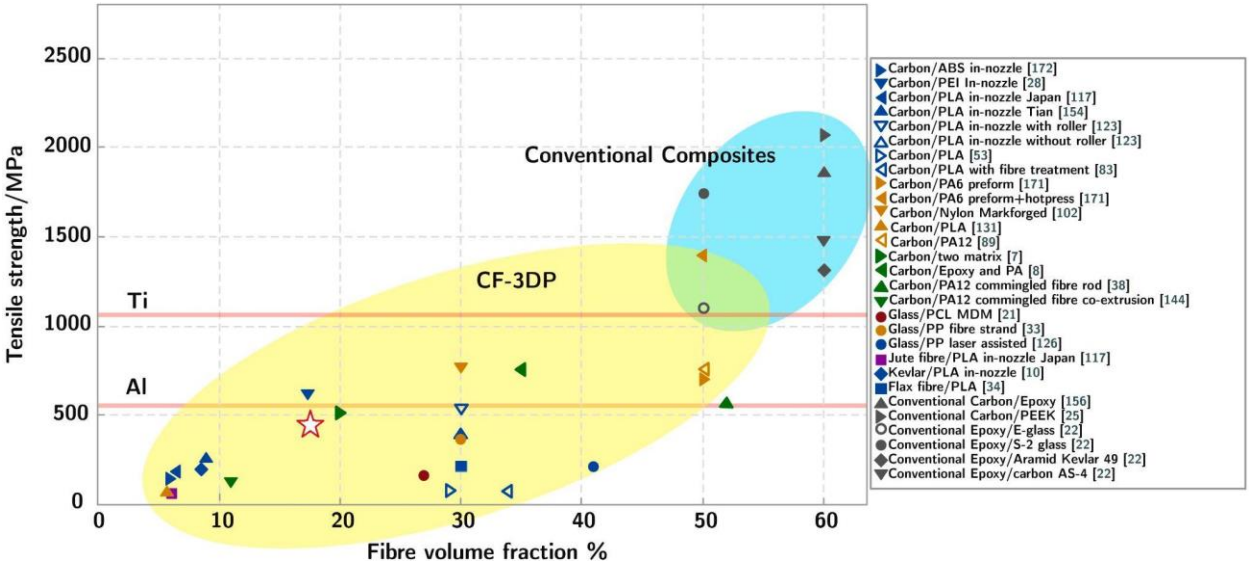

Figure 4.1. Contextualized tensile strength vs. V_{fiber} relationship of experimental 3D-Printed Continuous-fiber-reinforced composites ("CF-3DP") and conventional composites, data corresponding to the strength of Printed WDF and V_{fiber} = 18% was plotted as a red star filled by white. (Adapted from Zhuo et al., 2021)

From observing the location of Printed WDF data relative to others, it can be found that although its V_{fiber} is limited compared to many experimental continuous-fiber reinforced material systems, the strength is already comparable to the reference aluminum alloys' ultimate tensile strength, and surpassing most plotted material systems. The potential exist for Dyneema/PCL composite such that if 2 fiber tows of SK99 are fed through the filament manufacturing apparatus instead of 1 as what was investigated, the theoretical V_{fiber} will also double, which will

approximately double the strength of the printed filament to reach ~1000 MPa according to the ROM, a strength comparable to the reference ultimate tensile strength for stronger titanium alloys and entering the strength range of conventional composites. Moreover, if this trend can be extrapolated with 3 fiber tows, reaching a theoretical V_{fiber} of 54%, according to the ROM, the strength will approach 1500 MPa and surpass all of the experimental material systems on this graph, and become comparable to the strength of conventional Epoxy/carbon AS-4 composites (Tian et al., 2016). As the density of Dyneema fibers is only 0.975g/cm^3 and the density of PCL is only 1.13g/cm^3 (polymerdatabase.com, 2019), the resulting composite has a theoretical density of only 1.05 g/cm^3, even lower than the conventional Epoxy/carbon AS-4 composites at 1.46 g/cm^3 (Doleman, 2013).

The potential of Dyneema/PCL composites was evident from their mechanical properties. Yet, there were microstructural defects in the material—most notably, fiber waviness and non-uniform fiber distribution, leading to distinct fiber-rich and matrix-rich areas. These inconsistencies largely emanated from the filament-manufacturing apparatus and the specific conditions of the PCL bath including thermal inhomogeneity and possible mechanical misalignment. It was determined that to best preserve the fibers, the PCL bath was maintained at 70°C, only slightly above its melting point of 60°C. This low temperature induced low thermal conductivity for PCL, resulting in an uneven heat distribution in the bath. Entrapped air bubbles further intensified this inhomogeneity. The resultant spatial variations in temperature modulated the PCL's viscosity across the bath. When Dyneema fibers were pulled through high-viscosity zones, they encountered decreased mobility, leading to their dispersion in a more relaxed configuration and better matrix coating, as well as relative motion as compared to fibers passing through less viscous regions of the bath. This, in turn, introduced fiber waviness, an inherent

departure from the ideal linear alignment. Besides, induced residual stresses and non-uniform fiber distribution became more evident. Particularly in the Filament WDF samples, the fibers experienced intentional manipulations in the bath. Given the unbundled nature of the as-received Dyneema spool, these manipulations increased the variation in the fiber paths and consequently the waviness and uneven spatial distribution.

The fibers' trajectory as they were pulled through the nozzle significantly influenced their final orientation within the filament. If fibers were directed at angles deviating from the nozzle's central axis, it could lead to a preferential orientation on one side of the filament's cross-section. Such conditions were conducive to fiber waviness and an unbalanced matrix-to-fiber ratio in certain regions, since the deviation may change during the spooling process. Furthermore, observations made in conditions like a high bath temperature combined with increased spooling speeds which compromised the bath's viscosity and caused fibers to be separated from the filament as it exited the nozzle further proved this theory, such that the misalignment existed and varied during the filament manufacturing process, and caused the encapsulated fibers to adopt non-linear paths.

The stress-strain relationship plots, as seen in Figures 3.5 and 3.6, exhibit wave-like patterns indicative of premature failure of some Dyneema fibers in the tows and their composites. In the tows, some fibers might have pre-existing defects which were activated when the load was applied during testing. Another reason explaining these premature failures is that there was inevitable friction between the fibers and the fixture as they were in contact and relative motion as the tows deformed upon loading, intensifying the stresses in particular portions of these fibers. In Dyneema/PCL composites, this phenomenon can be attributed to insufficient load transfer, particularly severe in fiber-rich regions where fiber bundles form due to insufficient coating of the

fibers by the PCL (Oosterom et al., 2006). Additionally, some fibers were observed to be exposed, as evidenced in Figures 3.1 and 3.2. These exposed fibers are prone to fail at slightly lower global stress levels below the stress at fracture in the same fashion as Dyneema fiber tows, inducing a sudden load increase following a microscopically localized fracture, as the global stress continues to rise during a test. As a result, these premature failures cause samples to display lower stress at failure, since fewer fibers are left to bear the increasing load.

To address this issue, enhanced load-transfer mechanisms are proposed to promote the concurrent fracture of all fibers, potentially through improving the adhesion between the fiber and matrix, akin to the "sizing" approach used in carbon fiber composites. Furthermore, fiber pull-out tests can be utilized to evaluate interfacial shear strength (Chiu and Wang, 2004). Additionally, preventing microscopic fiber bundling and exposure is crucial for improving strength, especially for applications requiring a higher strength/modulus, such as aerospace applications, where a high fiber volume fraction is desirable (Zhuo et al., 2021).

The low slope of the stress-strain plot in the low-strain regime observed in Figure 3.5 for Dyneema can be attributed to fiber slack and misalignment in its pre-testing condition, a common occurrence for filament-type specimens in tensile tests as the load level is relatively low compared to the stress and strain at failure. The high-slope region more accurately depicts the real stress-strain behavior of the fiber tows.

A noteworthy aspect of the stress-strain behavior in Figure 3.6, mirrored from Figure 3.5, is the initial low-slope region. This is attributed to the globally elastic response of the composite, indicative of the slack present in these composite filaments, which was removed as the stress increased. As the stress increases during the tensile tests, there is a distinct transition point around 100 MPa. This differs significantly from what was observed for Dyneema fiber tows previously,

which shows a transition around 200-300 MPa. This discrepancy arises because compared to the fiber tows tested, the composite filaments only contained the same amount of strong and stiff fibers, but had much larger cross-sectional areas, as characterized by the low fiber volume fraction of 18%. However, the increase in stiffness of both fiber tows and composite filaments indicated the removal of slack of specimens, beyond which the measured stress-strain responses more closely reflect the actual load bearing performance of the tested specimens. When strained to around 2%, Dyneema nears its maximum strain level, making premature failures more likely than at lower strain levels. As the load and deformation further intensified, the composite commenced its yielding phase, reflected in a decreasing slope of the stress-strain plot (Courtney, 2005). It is worth noting that such a yielding response is not present in examined Dyneema fiber tows. This is because these fiber tows are not braided and do not possess inherently effective mechanisms to transfer loads among unevenly stressed fibers. However, in the composite form, the PCL matrix, if adequately interspersed between fibers, can evenly distribute the load among fibers through interfacial shear forces, up to the interfacial shear strength between fibers and the matrix (Swolfs et al., 2015). As the interfacial shear strength was reached, the matrix would be moving with respect to the fibers and cause the fibers to be pulled out. The revealed fibers at elevated loading levels would then fracture because of slightly uneven load, immediately followed by the global filament failure. If the interfacial strength was strong enough, the filaments would fail in the fiber fracture fashion, instead of the fiber pull-out fashion, which was observed in this study for composite samples other than the Printed WDF type. The fiber pull-out phenomenon at maximum load and stress levels explains the yielding observed in stress-strain curves corresponding to composite samples within which relatively efficient load transfer through fiber/matrix interfaces were present. For Printed WDF samples, the fracture was dominant by the relative extent of fiber

exposure, as they lacked effective load transfer mechanisms provided by satisfactory matrix inclusion and sufficient fiber/matrix interface, premature failures are more likely to occur and induce sudden load change, at load levels close to the maximum stress of Dyneema fibers, such changes can also induce immediate fracture of other fibers, making yielding impossible. For these samples, axial fiber-pullouts were not present. Instead, debonding of surface fibers and fiber breakage of internal fibers were observed.

When placing the strengths of Dyneema fiber tows adjacent to their composite products as presented in Figure 3.7 a), a stark contrast is evident. The composites showcase markedly reduced stresses at failure. A critical contributor can be traced back to their low fiber volume fraction. This is intrinsically tied to the equipment used during their fabrication – notably, the choice of the nozzle size at the exit of the PCL bath tank of the filament-producing apparatus, noting that its cross-sectional area was 0.502 mm^2 compared to the 0.0903 mm^2 cross-sectional area of the fiber tow. Due to this selection, the resultant composites possess cross-sectional areas that vastly overshadow those of the Dyneema fiber tows, as shown in Figure 3.1.

Further diving into the intricacies of this reduced strength, particularly among the printed filaments compared to pre-printed raw filaments, offers more insights. The core of this vulnerability lies in the damage inflicted upon the embedded Dyneema fibers during the printing process. Their structure, specifically the crystallinity, undergoes significant degradation due to elevated temperature at the printer nozzle. This observation is particularly pronounced for the WDF samples. The following section delves deeper into this structural deterioration, elucidating the precise mechanisms and consequences.

A comparative analysis of strain at failure across various sample types, as depicted in Figure 3.7b), reveals a fascinating trend. The composite strains predominantly surpass Dyneema's

values, with a notable exception being the Printed WDF. The trend can be attributed to the yielding effect of composites as the stresses approach the fracture, as shown in Figure 3.6. The anomaly found in the Printed WDF samples can be traced back to the micrographs in Figure 3.2, which clearly highlight a significant number of fibers being directly exposed, devoid of the matrix PCL. Such an exposure undermines the load-bearing capacity of the fibers, primarily due to the lack of effective load-transfer mechanisms (Swolfs et al., 2015).

Continuing with the Printed WDF samples, the root cause of such exposure lies in the very printing process. Its continuity hinges on filament adhesion right after it passes through the printer nozzle, either adhering to the printer bed or the layer beneath. Concurrently, the viscous molten PCL flows downward due to gravity. These conditions exert tension in the Dyneema fibers, making them inclined towards the printer nozzle, which remains heated at a precarious 120°C, not much lower than their melting points between 144°C and 152°C (FibrXL, 2020). Given that the recommended service temperature for Dyneema is only 70°C, this heightened temperature exposure critically jeopardizes the tenacity and modulus of the fibers (FibrXL, 2020). After the composite cools down as a part of the printed structure, damaged fibers are exposed as the matrix PCL solidifies underneath.

This vulnerability becomes even more pronounced in larger printed structures. For instance, as showcased in Figures 3.3 and 3.4, the fiber exposure is alarmingly exacerbated at points where the printer nozzle alters its trajectory. Notably, during these turning points, the printing speed plunges from 100mm/min to a mere 10mm/min. This deceleration, combined with the printer nozzle pressing onto the deposited layer to augment the molten PCL pool for better adhesion and prevent the new layer to be stripped away as fibers are in tension, increases the thermal exposure duration. Such extended exposures undermine the fiber structure by reducing its crystallinity and

consequently its strength (thermal damage reference). Therefore, these turning points in printed structures larger than single-layer and single-path filaments are potential crack initiators.

Nevertheless, not all printed samples experience such vulnerabilities. While both Printed WDF and Printed WODF undergo the printing process, the latter suffers minimal degradation. This resilience can be traced back to the placement of the Dyneema fibers, predominantly located near the center of the filament, as shown in Figure 3.1 b), and remain shielded when passing through the hot printer nozzle. Moreover, the inherent heat capacity and minimal heat transfer of PCL further protect the majority of fibers from heat.

Compared to more straightforward stress and strain values, toughness, as presented in Figure 3.8 is a multifaceted material property. It relies not only on a material's ability to bear loads, represented by strength but also on its capacity to deform, depicted by strain. For composites, this property is important as high toughness can prevent catastrophic failure of the material while not increasing the weight (Ichihara and Ueda, 2023). Ideally, a simultaneous enhancement in both strength and strain is sought. However, a significant boost in one, even at the expense of the other, can still be acceptable. One strategy to enhance toughness involves optimizing the protective role of the matrix around fibers. This could be achieved by fine-tuning the microstructure and processing conditions, which in turn can benefit the apparent fiber strength (AFS). A potential method to achieve this is by ensuring uniform coating on each fiber strand. One way to do this might be to individually feed the fiber strands into the PCL bath, closely resembling the commercial pultrusion apparatus setup, as shown in Figure 2.1 (Minchenkov et al., 2021). This method could also present an opportunity to control the fiber volume fraction within the composite, potentially further optimizing the composite's mechanical properties.

Furthermore, promoting uniform load distribution within the composite is paramount. Strengthening the chemical bonding between the fiber and matrix could facilitate this. A common method employed to enhance this bond is by applying "sizing" to the fibers before they are introduced into the bath, as proven to be effective for carbon-fiber-reinforced polymers in the industry. This improves the mechanical interlocking of the fibers with the matrix. Another riskier approach involves altering the fiber's surface chemistry and topography via etching to boost interface bonding at a molecular level (Chhetri and Bougherara, 2021). Similarly, decreasing the viscosity of the matrix polymer bath by means of blending or additives may exert both desirable and undesirable changes, such that low viscosity at low temperatures can help better coat individual fibers in the filament-manufacturing process, but may leave fibers unprotected after being melted by the excessive heat during the printing process.

While current evaluations, especially the AFS, presented in Figure 3.9, show that fibers are largely preserved in the composite and match the properties of untreated Dyneema fiber tows, the AFS for Printed WDF composites presents a concern. The printing process subjected fibers in these samples to high temperatures while significantly exposed, leading to significant thermal damage. As this fiber configuration more closely resembles the realistic structure of composites subjected to mechanical loading, with fibers more evenly distributed within the matrix to minimize fiber agglomerations and matrix-rich areas, fully exploiting its potential may lead to facilitated large-scale production for various applications.

Analyzing the Weibull analysis data, as shown in Figure 3.10, reveals a clear trend: the more the fibers undergo processing to become composites, the less reliable they become. One notable observation is the significantly reduced reliability of Printed WDF compared to any other type of samples, owing to the extensive thermal damage fibers underwent during printing. This

emphasizes the intricate interplay between microstructure, processing conditions, and the resultant properties of the composite.

Several factors can influence the extent of this thermal damage. For instance, the temperature at the nozzle during printing, the distribution of fibers within the filament as it passes through the nozzle, the fiber volume fraction, and the spatial positioning of fibers in the filament's cross-section. Many of these factors are tied to specific settings and intricacies of the filament production apparatus and process.

This scenario is reminiscent of the challenges faced in traditional composite production methods. Structural defects can accumulate over the various stages of a complicated manufacturing process, ultimately compromising the composite's performance and reliability. Ensuring optimal composite properties, therefore, demands meticulous monitoring of the entire production process and following the best practices closely. Only by identifying and addressing potential sources of variability and errors early on, consistent and high-quality composite parts can be manufactured.

Chapter 5 - Conclusions and Future Work

5.1 Conclusions

In this document, a novel composite filament composed of continuous Ultra-High Molecular Weight Polyethylene (UHMWPE) fibers and polycaprolactone (PCL) with high strength at low fiber volume fraction was developed for Fused Deposition Modeling. After evaluating the viability of the manufacturing process and printability of the filament, the structure-property relationship was established, accompanied by an identification of the most influential processing parameters, namely fiber dispersion and temperature. It can be concluded that this material has the potential to be used as the next generation of flexible impact-resistant protection, which can be used in aerospace and explosion protection industries.

The investigation included the assessment of two approaches for fabricating filaments in terms of their ability to produce composite filaments for FDM with consistent properties. The microstructure and mechanical properties of the continuous UHMWPE fibers and composite filaments were characterized. Both demonstrated the superior printability of these composite filaments as they were produced with a pultrusion-style impregnation approach instead of a co-extrusion style. The microstructure of the filaments with dispersed fibers revealed fiber exposure, which consequently caused property degradation during printing with a reduction of nearly 20% in apparent fiber strength (AFS), compared to the fibers in their as-received condition. The AFS corresponding to fibers in the printed condition without intentional dispersion manipulation achieved a slight increase in AFS of 3.2%, indicating that compared to the fiber tows, the load transfer mechanism and thermal protection provided by the matrix in the composite exerted a strengthening influence on a similar degree compared to the weakening influence exerted from thermal damage experienced by the fibers during printing. The strength of printed filaments was

474±62 MPa and 548±46 MPa for those with dispersed fibers and without dispersed fibers, respectively. From Weibull analysis, it was concluded that both the reliability and characteristic strength are negatively impacted by the printing process, and this effect was exacerbated by the dispersed fiber configuration.

Although the fiber volume fraction of the developed composite was relatively low compared to others found in the literature and industrial materials, it exhibits exceptional strength and has the potential to reach or even surpass the strength of conventional carbon-fiber-reinforced composites. It would be simple to introduce multiple fiber tows into the matrix bath during filament manufacturing to achieve higher volume fraction.

In summary, these results are clearly the first of their kind regarding the processing-structure-properties of compliant continuous-fiber-reinforced high-performance composites, which could expand the FDM method and diversify the material options that can be manufactured. Although defects and low fiber volume fraction would hinder immediate wide adoption, there exists great potential for fine-tuning the properties according to specific applications. The successful development of this composite filament further advanced the polymer composites reinforced by continuous fibers, and the unlimited possibilities for selecting materials for additive manufacturing.

5.2 Future work

The research presented in this thesis has elucidated the potential for developing and printing UHMWPE/PCL composites by FFF. However, there are still various aspects of research that need further exploration to improve its performance. As such, a significant opportunity lies in the modification of the fiber-matrix interface. By altering the fiber surface through methods like plasma treatments or etching, mechanical and chemical interlocking between the UHMWPE fibers

and the matrix can be augmented. The resulting strengthened interface can more effectively distribute the load evenly, preventing premature failures, improving the reliability, and increasing the strength of the composite. Moreover, the strengthened interface allows for better fiber integration within the matrix, thus improving printability and offering more structural integrity and design freedom.

A much more straightforward approach for improving the strength of these composites is to increase the fiber volume fraction within the composite. However, this may induce problems in printability and incomplete fiber impregnation while it is fed through the filament-manufacturing apparatus. The correlation between increased fiber volume fraction and strength may reach a maximum beyond which the weakening dominates, as more defects are present in the composites, and effective load transfer cannot be realized.

To prevent fiber damage and also the formation of weak matrix-rich regions, controlled dispersion of fibers within the composite is highly recommended for future research. The fiber placement method developed in this research will be beneficial for many other composites, especially for those reinforced by continuous fibers.

References

Amza, C.G., Zapciu, A., Eyþórsdóttir, A., Björnsdóttir, A., Borg, J., Embedding ultra-high-molecular-weight polyethylene fibers in 3D-printed polylactic acid (PLA) parts, Polymers. 11 (2019) 1825. doi:10.3390/polym11111825.

Marquis, C., Song, R., Waddell, S., Luong, A. Arola, D., Additive Manufacturing with Continuous Ultra-High Molecular Weight Polyethylene Yarn, Materials & Design. (2023). (Under review)

Avient, "Dyneema® Fiber The world's strongest fiberTM," Dyneema® fiber, https://www.dyneema.com/our-products/dyneema-fiber (accessed Jul. 29, 2023).

Chhetri, S., Bougherara, H., A comprehensive review on surface modification of UHMWPE fiber and interfacial properties, Composites Part A: Applied Science and Manufacturing. 140 (2021) 106146. doi:10.1016/j.compositesa.2020.106146.

Chiu, H.-T., Wang, J.-H., The relationship between Zeta-potential and pull-out shear strength on modified UHMWPE fiber reinforced epoxy composites, Polymer Composites. 19 (1998) 347–351. doi:10.1002/pc.10107.

Courtney, T.H., Mechanical Behavior of Materials: Second Edition, Waveland Press, Long Grove, Illinois, 2005.

Doleman, B., Thermal Characterization Of AS4/3501-6 Carbon-Epoxy Composite, thesis, North Carolina Agricultural and Technical State University, 2013.

Fereiduni, E., Ghasemi, A., Elbestawi, M., Selective laser melting of aluminum and titanium matrix composites: Recent progress and potential applications in the aerospace industry, Aerospace. 7 (2020) 77. doi:10.3390/aerospace7060077.

FibrXL, "Dyneema®," FibrXL, https://fibrxl.com/fibrxl-performance/fibers/dyneema/ (accessed Jul. 29, 2023).

Fu, S.-Y., Lauke, B., Effects of fiber length and fiber orientation distributions on the tensile strength of short-fiber-reinforced polymers, Composites Science and Technology. 56 (1996) 1179–1190. doi:10.1016/s0266-3538(96)00072-3.

Hu, Q., Duan, Y., Zhang, H., Liu, D., Yan, B., Peng, F., Manufacturing and 3D printing of continuous carbon fiber prepreg filament, Journal of Materials Science. 53 (2017) 1887–1898. doi:10.1007/s10853-017-1624-2.

Ichihara, N., Ueda, M., 3D-printed high-toughness composite structures by anisotropic topology optimization, Composites Part B: Engineering. 253 (2023) 110572. doi:10.1016/j.compositesb.2023.110572.

Kainer, K.U., Basics of Metal Matrix Composites, in: Metal Matrix Composites Custom-Made Materials for Automotive and Aerospace Engineering, 1st ed., Wiley-VCH, Weinheim, Germany, 2006: pp. 1–54.

Karalekas, D.E., Study of the mechanical properties of nonwoven fibre mat reinforced photopolymers used in rapid prototyping, Materials & Design. 24 (2003) 665–670. doi:10.1016/s0261-3069(03)00153-5.

Material Sample Shop, "Polycaprolactone (PCL) - a polymer with a very low melting point," Material Sample Shop, https://www.materialsampleshop.com/products/polycaprolactone (accessed Jul. 29, 2023).

Matsuzaki, R., Nakamura, T., Sugiyama, K., Ueda, M., Todoroki, A., Hirano, Y., Yamagata, Y., Effects of set curvature and fiber bundle size on the printed radius of curvature by a continuous carbon fiber composite 3D printer, Additive Manufacturing. 24 (2018) 93–102. doi:10.1016/j.addma.2018.09.019.

Minchenkov, K., Vedernikov, A., Safonov, A., Akhatov, I., Thermoplastic pultrusion: A Review, Polymers. 13 (2021) 180. doi:10.3390/polym13020180.

Mori, K., Maeno, T., Nakagawa, Y., Dieless forming of carbon fibre reinforced plastic parts using 3D printer, Procedia Engineering. 81 (2014) 1595–1600. doi:10.1016/j.proeng.2014.10.196.

Oosterom, R., Ahmed, T.J., Poulis, J.A., Bersee, H.E.N., Adhesion performance of UHMWPE after different surface modification techniques, Medical Engineering & Physics. 28 (2006) 323–330. doi:10.1016/j.medengphy.2005.07.009.

Pierson, H.A., Celik, E., Abbott, A., De Jarnette, H., Sierra Gutierrez, L., Johnson, K., Koerner, H., Baur. J., Mechanical properties of printed epoxy-carbon fiber composites, Experimental Mechanics. 59 (2019) 843–857. doi:10.1007/s11340-019-00498-z.

polymerdatabase.com, "Poly(caprolactone)," Polymer Database, https://polymerdatabase.com/polymers/polycaprolactone.html (accessed Aug. 8, 2023).

Rios, O., Carter, W., Post, B., Lloyd, P., Fenn, D., Kutchko, C., Rock, R., Olsen, K., Compton B., 3D printing via ambient reactive extrusion, Materials Today Communications. 15 (2018) 333–336. doi:10.1016/j.mtcomm.2018.02.031.

Rosa, D.S., Neto, I.C., Calil, M.R., Pedroso, A.G., Fonseca, C.P., Neves, S., Evaluation of the thermal and mechanical properties of poly(?-caprolactone), low-density polyethylene, and their blends, Journal of Applied Polymer Science. 91 (2004) 3909–3914. doi:10.1002/app.13596.

Safari, F., Kami, A., Abedini, V., 3D printing of continuous fiber reinforced composites: A review of the processing, pre- and post-processing effects on mechanical properties, Polymers and Polymer Composites. 30 (2022) 096739112210987. doi:10.1177/09673911221098734.

Saito, Y., Fernandez, F., Tortorelli, D.A., Compel, W.S., Lewicki, J.P., Lambros, J., Experimental validation of an additively manufactured stiffness-optimized short-fiber reinforced composite clevis joint, Experimental Mechanics. 59 (2019) 859–869. doi:10.1007/s11340-019-00514-2.

Sano, Y., Matsuzaki, R., Ueda, M., Todoroki, A., Hirano, Y., 3D printing of discontinuous and continuous fibre composites using stereolithography, Additive Manufacturing. 24 (2018) 521–527. doi:10.1016/j.addma.2018.10.033.

Seetharaman, S., Gupta, M., Additive manufacturing of Metal Matrix Composites, Encyclopedia of Materials: Composites. 1 (2021) 209–229. doi:10.1016/b978-0-12-819724-0.00099-9.

Swolfs, Y., Verpoest, I., Gorbatikh, L., Issues in strength models for unidirectional fibre-reinforced composites related to Weibull distributions, fibre packings and boundary effects, Composites Science and Technology. 114 (2015) 42–49. doi:10.1016/j.compscitech.2015.04.002.

Tekinalp, H.L., Kunc, V., Velez-Garcia, G.M., Duty, C.E., Love, L.J., Naskar, A.K., Blue, C. A., Ozcan, S., Highly oriented carbon fiber–polymer composites via additive manufacturing, Composites Science and Technology. 105 (2014) 144–150. doi:10.1016/j.compscitech.2014.10.009.

Tian, X., Liu, T., Yang, C., Wang, Q., Li, D., Interface and performance of 3D printed continuous carbon fiber reinforced PLA composites, Composites Part A: Applied Science and Manufacturing. 88 (2016) 198–205. doi:10.1016/j.compositesa.2016.05.032.

Tian, X., Todoroki, A. Liu, T., Wu, L., Hou, Z., Ueda, M., Hirano, Y., Matsuzaki, R., Mizukami, K., Iizuka, K., Malakhov, A. V., Polilov, A. N., Li, D., Lu, B., 3D printing of continuous fiber reinforced polymer composites: Development, application, and prospective, Chinese Journal of Mechanical Engineering: Additive Manufacturing Frontiers. 1 (2022) 100016. doi:10.1016/j.cjmeam.2022.100016.

Ueda, M., Kishimoto, S., Yamawaki, M., Matsuzaki, R., Todoroki, A., Hirano, Y., Le Duigou, A., 3D compaction printing of a continuous carbon fiber reinforced thermoplastic, Composites Part A: Applied Science and Manufacturing. 137 (2020) 105985. doi:10.1016/j.compositesa.2020.105985.

van de Werken, N., Tekinalp, H., Khanbolouki, P., Ozcan, S., Williams, A., Tehrani, M., Additively manufactured carbon fiber-reinforced composites: State of the art and perspective, Additive Manufacturing. 31 (2020) 100962. doi:10.1016/j.addma.2019.100962.

Wen, S., Shin, Y.C., Modeling of transport phenomena in direct laser deposition of metal matrix composite, International Journal of Heat and Mass Transfer. 54 (2011) 5319–5326. doi:10.1016/j.ijheatmasstransfer.2011.08.011.

Wickramasinghe, S., Do, T., Tran, P., "FDM-based 3D printing of Polymer and associated composite: A review on mechanical properties, defects and treatments," Polymers. 12 (2020) 1529. doi:10.3390/polym12071529.

Yan, C., Hao, L., Xu, L., Shi, Y., "Preparation, characterisation and processing of carbon fibre/polyamide-12 composites for Selective Laser Sintering," Composites Science and Technology. 71 (2011) 1834–1841. doi:10.1016/j.compscitech.2011.08.013.

Zhang, Z., Long, Y., Yang, Z., Fu, K., Li, Y., "An investigation into printing pressure of 3D printed continuous carbon fiber reinforced composites," Composites Part A: Applied Science and Manufacturing. 162 (2022) 107162. doi:10.1016/j.compositesa.2022.107162.

Zhang, M., Tian, X., Li, D., "Interfacial transcrystallization and mechanical performance of 3D-printed fully recyclable continuous fiber self-reinforced composites," Polymers. 13 (2021) 3176. doi:10.3390/polym13183176.

Zhuo, P., Li, S., Ashcroft, I. A., Jones, A. I., "Material extrusion additive manufacturing of continuous fibre reinforced polymer matrix composites: A review and outlook," Composites Part B: Engineering. 224 (2021) 109143. doi:10.1016/j.compositesb.2021.109143.